PhD Thesis / Tesi Doctoral

-

INTRATHECAL ADMINISTRATION OF AAVrh10 CODING FOR β-GLUCURONIDASE CORRECTS BIOCHEMICAL AND HISTOLOGICAL HALLMARKS OF MUCOPOLYSACCHARIDOSIS TYPE VII MICE AND IMPROVES BEHAVIOR AND SURVIVAL

Author / Autora:

Gemma Pagès i Pi

Director / Directora:

Assumpció Bosch Merino

Doctorat en Bioquímica, Biologia Molecular i Biomedicina
Departament de Bioquímica i Biologia Molecular
Universitat Autònoma de Barcelona

2015

RESULTS

RESULTS

Since MPS VII mice are very valuable and difficult to breed, we decided to choose the vector and the administration route before starting the assays with MPS VII mice. With this purpose, we performed several experiments in wild type mice using vectors that express the GFP reporter gene. In addition, we did a pilot study with the chosen vector and administration route in MPS VII mice, in order to fine-tune the approach. Hence, the results of this work are divided in the following parts:

1. **AAV9 and AAVrh10 efficiency, tropism and immune response in WT mice**
   - 1.1. Intravenous administration of AAV9 and AAVrh10
   - 1.2. Innate mmune response after IV administration of AAV9 and AAVrh10
   - 1.3. Intrathecal administration of AAVrh10: brain and liver transduction

2. **Gene therapy to treat MPS VII mice: intrathecal administration of AAVrh10-GUSB in MPS VII mice**
   - 2.1. Intrathecal AAVrh10-GUSB in MPS VII mice. Pilot Study.
   - 2.2. Intrathecal AAVrh10-GUSB in MPS VII mice. Biochemical, histological, behavioral and survival effects of short- and long-term treatment.

1. AAV9 AND AAVrh10 EFFICIENCY, TROPISM AND IMMUNE RESPONSE IN WILD TYPE MICE

This part of the work is focused in choosing the ideal viral vector and administration route for the gene therapy approach for MPS VII. Previous published data demonstrated that intravenous delivery of AAV9 targets the CNS in adult mice (Foust et al. (2009)), and IV AAVrh10 also transduced the brain in neonates (Hu et al. (2010)). However, CNS transduction in adult mice after IV delivery of AAVrh10 had not been characterized. Moreover, we had previously shown that intrathecally administered AAVrh10 transduced sensory and motor neurons in a similar manner than AAV9 (Homs et al. (2014), Snyder et al. (2011)), while the efficiency of brain and somatic organs transduction by intrathecal delivery in mice remained to be elucidated.

1.1. INTRAVENOUS ADMINISTRATION OF AAV9 AND AAVrh10

Since IV AAVrh10 transduction of the CNS had not been characterized, we wanted to compare the transduction patterns of AAV9 and AAVrh10 after IV delivery in our hands. With this aim, 1.94 x 10^{12} vg of either AAV9 or AAVrh10 coding for GFP under the control of the CAG promoter, were injected via tail vein to 8-week-old ICR mice (3 mice per group). Mice were sacrificed three weeks postadministration, tissues were fixed, and direct GFP signal was visualized in liver, DRG, SC and brain samples (**Figure 16**).

GFP expression in liver was widespread using both AAV serotypes, and we observed that AAV9-injected mice exhibited higher signal intensity than AAVrh10 (**Figure 16A and 16B**). Therefore, since the expression cassette is the same in both vectors, AAV9 appeared to be more efficient in transducing cells in the liver than AAVrh10.

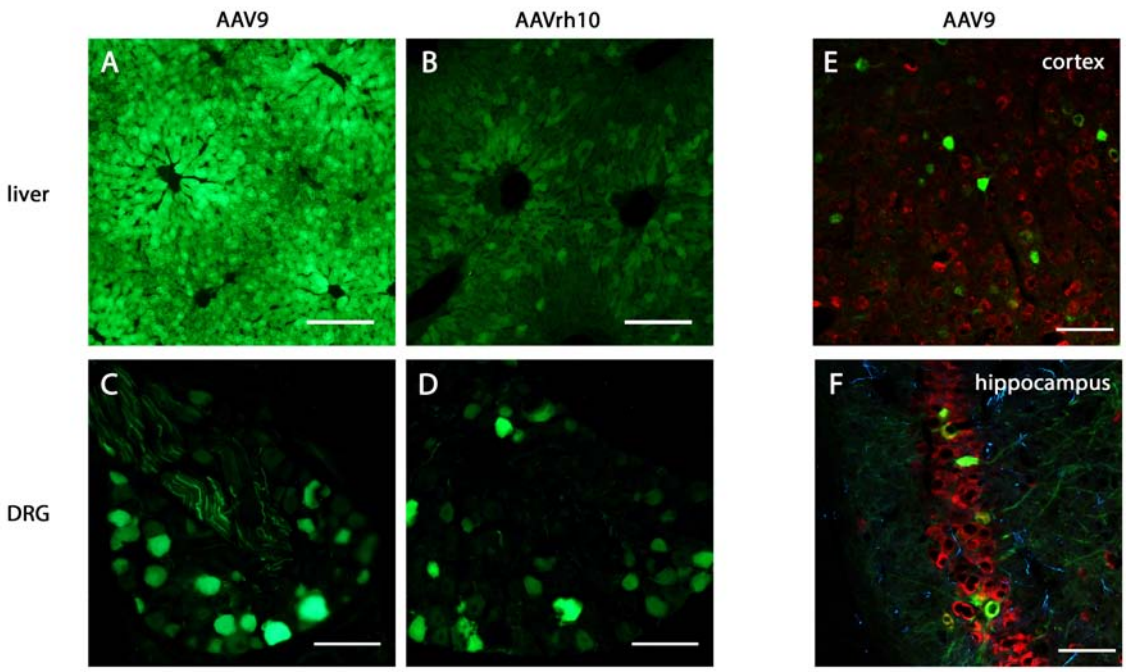

Figure 16: Intravenous administration of AAV9 and AAVrh10. Direct GFP signal in green; NeuN staining in red; GFAP staining in blue. (**A, B**) Liver transduced by AAV9 (A) and AAVrh10 (B). Scale bar: 200 μm (**C, D**) DRG transduced by AAV9 (C) and AAVrh10 (D). Scale bar: 100 μm (**E, F**) Brain structures transduced by AAV9: cortex (E) and hippocampus (F). Scale bar: 70 μm.

In the analysis of samples from nervous system, dorsal root ganglia presented GFP transduced neurons using both AAV serotypes, without apparent differences in the number of cells or the intensity of the GFP signal of the sensory neurons (**Figure 16C and 16D**). Spinal cord slices showed GFP fluorescence only in the dorsal sensory tracts formed by the axons of the transduced DRG neurons, without any GFP signal in the SC grey matter that contains the motor neuron nuclei (not shown). Finally, when analyzing sagittal brain slices, we scarcely observed transduction in the AAVrh10-injected mice (data not shown), whereas we found GFP signal in different areas of the AAV9-injected brains. Among other areas, we saw GFP-expressing neurons in the hippocampus (**Figure 16E**) and in the cortex (**Figure 16F**). Hence, concerning the NS, both AAV9 and AAVrh10 are capable to cross the BBB and access the nervous system. Both AAV serotypes are capable to transduce DRG neurons but not motor neurons in the spinal cord. And in brain, AAV9 is clearly more efficient than AAVrh10 in reaching and transducing cells.

In conclusion, with an intravenous injection of 1.94 x 10^{12} vg per mouse, AAV9 appears to be more efficient than AAVrh10 in transducing cells in liver and brain, while both serotypes are capable to transduce sensory neurons but not motor neurons.

1.2. INNATE IMMUNE RESPONSE AFTER IV ADMINISTRATION OF AAV9 AND AAVrh10

In viral gene therapy trials, transduction efficiency can be impaired due to the preexisting NAbs, acquired by natural AAV infections and present in serum or CSF of patients. Naive mice do not present preexisting Nabs against AAVs, therefore in preclinical trials the first administration of the viral vector would not be affected by immunity. Nonetheless, this first administration could raise NAbs that could interfere in the transduction in case of a readministration paradigm of gene therapy, which is also important in human patients. Therefore the immunogenicity of the vector should be taken into account, and the choice of an AAV serotype that raises low levels of NAb is important in the first steps of the design of gene therapy strategies.

In this work we compared the immunogenicity of AAV9 and AAVrh10 in mice, first by quantifying via indirect ELISA the total IgGs anti-AAV raised three weeks after intravenous injection of 10^{11} vg per mouse of each virus, and then by testing the sera's capacity to neutralize the virus using a luciferase reporter gene (**Figure 17**).

Figure 17A shows that animals injected with AAV9 raised more IgGs anti-AAV than animals injected with AAVrh10 (t test $p < 0.05$). Note that in normal mouse sera the typical IgG concentration range is 0.7-5 mg/ml. Thus, our quantification of the IgGs anti-AAV subpopulation is physiologically compatible. **Figure 17B** demonstrates that sera with antibodies raised against AAV9 are more neutralizing than with antibodies against AAVrh10. The percentage of infection inhibition dropped significantly for AAVrh10 over a series of serum dilutions, whereas for AAV9 it remained nearly 100% throughout. The mean percentage of infection inhibition comparing AAVrh10 and AAV9 at 1:200 serum dilution is seen in **Figure 17C**, which may be directly compared

with IgGs anti-AAV raised (**Figure 17A**). Pearson correlation analysis showed a significant positive correlation between IgGs and NAbs (0.776, $p = 0.0002$, $N = 17$).

These results indicate that, regarding the propensity to raise NAbs in mice, AAVrh10 is a more favorable choice of vector than AAV9, raising fewer antibodies in the context studied.

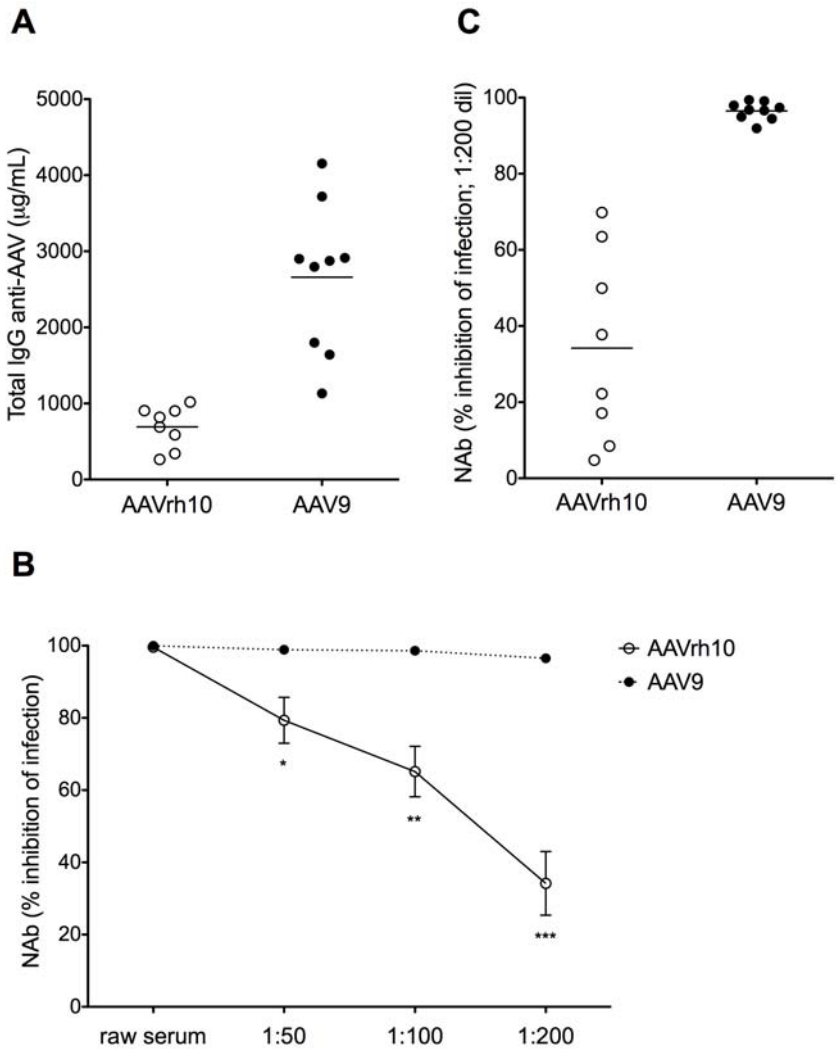

Figure 17: Immunogenicity of AAV9 and AAVrh10 in mice after IV injection of 10^{11} vg/ml of either AAV9 (n=9) or AAVrh10 (n=8). All samples tested in duplicate. (**A**) Total IgG anti-AAV µg/ml determined by indirect ELISA, — denotes the mean. (**B**) Neutralizing antibodies expressed as percentage of inhibition of AAV infection of HEK293 cells by the sera over a dilution range, determined using a luciferase reporter gene. Statistics: *t*-tests; *$p < 0.05$, ** $p < 0.01$, *** $p < 0.001$. (**C**) Scatter plot of NAb data at 1:200 dilution from (B), — denotes the mean.

1.3. INTRATHECAL ADMINISTRATION OF AAVrh10: BRAIN AND LIVER TRANSDUCTION

Previous work published by our group showed that AAVrh10 delivered intrathecally in ICR mice was capable to efficiently transduce sensory and motor neurons with a dose of 10^{11} vg per mouse as a potential strategy for diabetic neuropathy treatment (Homs et al. (2014)). This dose is 20 times lower than the dose we administered intravenously but as it was confined to the CSF, the treatment was efficient enough. In order to test whether this strategy was suitable for MPS VII treatment, we needed to check whether the intrathecal injection of AAVrh10 was also capable to efficiently transduce brain and also peripheral organs such as liver. Hence, we injected intrathecally, by lumbar puncture, 10^{11} vg of AAVrh10-GFP per mouse, in 8-week-old ICR mice (n = 4), and brain and liver samples were harvested after three weeks.

Figure 18 shows the liver transduction achieved by intrathecal administration of AAVrh10-GFP, detected by direct GFP fluorescence. The cells that are closer to central veins in liver parenchyma exhibit higher GFP signal, suggesting that the viral vector arrived to the liver via bloodstream. Thus, as previously described for many AAV serotypes (Towne et al. (2009), Samaranch et al. (2012), Haurigot et al. (2013), Gray et al. (2013)), AAVrh10 injected in the CSF is drained to the blood circulation and it is capable to transduce peripheral tissues. Interestingly, the magnitude of the liver transduction achieved by intrathecal injection of AAVrh10 is similar to the transduction seen after the intravenous administration of this vector, delivering a much lower dose. (**Figure 16B**)

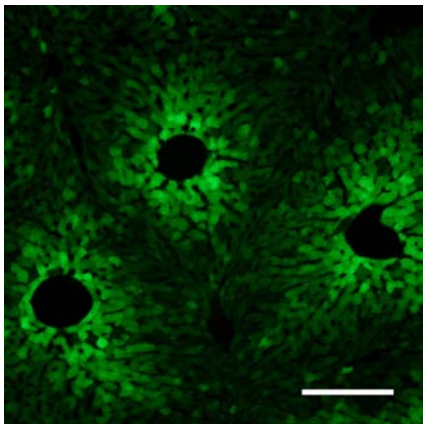

Figure 18: Liver transduction 3 weeks after intrathecal administration of 10^{11} vg of AAVrh10-GFP. Direct GFP signal. Scale bar: 200 μm.

Concerning the CNS, we observed that intrathecal AAVrh10 was able to reach and transduce cells in different areas of the brain (**Figure 19**).

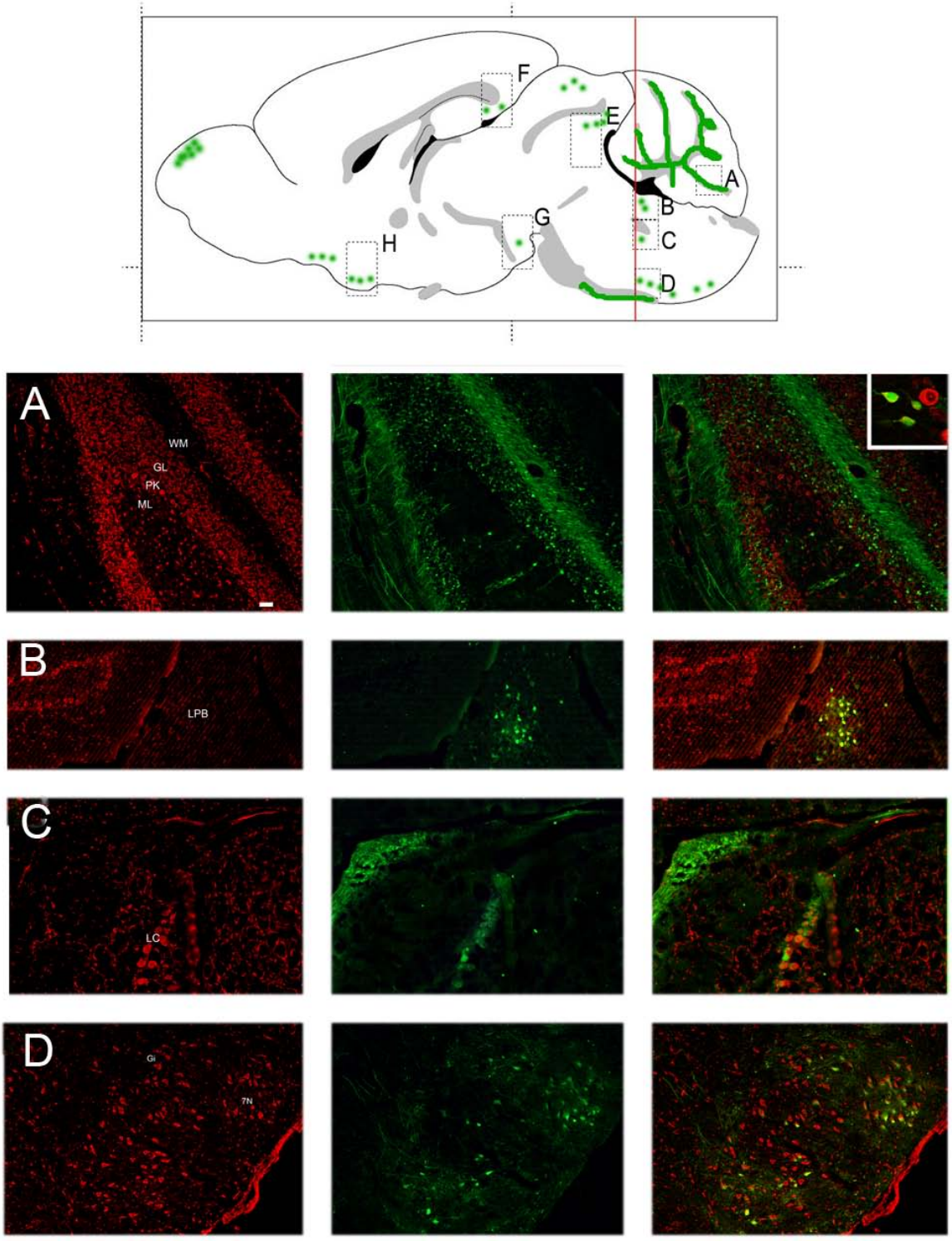

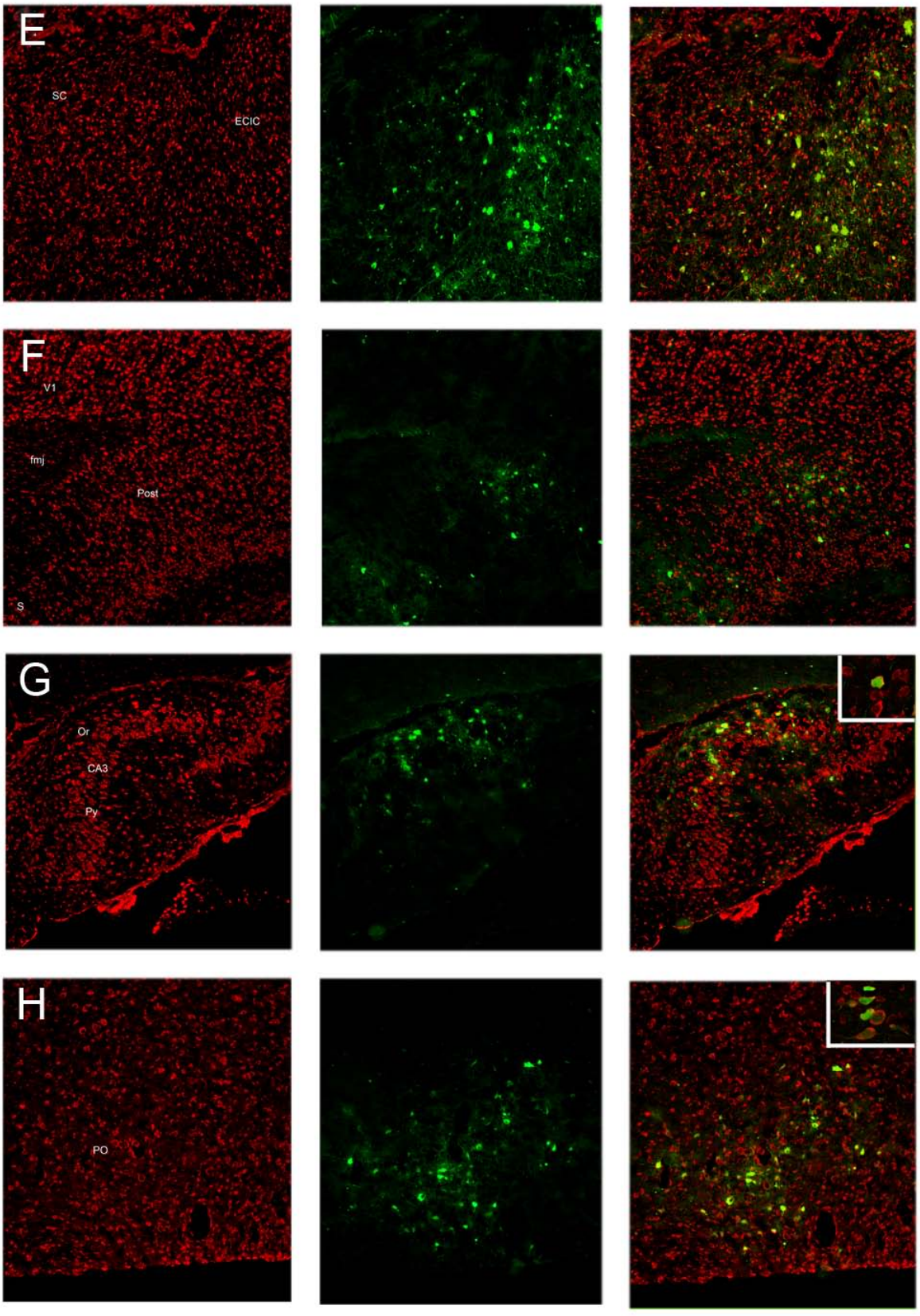
E
SC
ECIC
F
V1
fmj
Post
S
G
Or
CA3
Py
H
PO

Figure 19: Brain transduction after intrathecal injection of 10^{11} vg of AAVrh10-GFP. **Scheme:** drawing of a brain sagittal section. Squares mark the region shown in each labeled microphotograph representing different areas distributed along the brain. Green dots and lines where the strongest GFP-positive staining was observed have been also highlighted in green onto the brain diagram. A red line crossing the cerebellum and brainstem indicates the level where the structures are shown in pictures A-D. **Pictures:** microphotographs of coronal (**A-D**) or sagittal (**E-H**) brain sections at different levels. Panels in red show fluorescent-Nissl staining of neurons and in green the corresponding GFP expression. (**A**) Coronal section of the cerebellum showing the molecular (ML), granular (GL) and Purkinje cell layers (PK). Note extensive GFP-positive staining of fibers in the white matter (WM) and in terminal ends in the GL. (**B**) Several GFP-positive neurons in the lateral parabranchial nuclei. (**C**) Most neurons in the locus coeruleus are GFP-positive. (**D**) Somas and processes of gigantocellular neurons (Gi) at the reticular nuclei as well as motor neurons of the facial nucleus (7N) presented strong GFP signal. (**E**) At the external cortex of the inferior (ECIC) and superior colliculum (SC) several neurons and terminals show GFP expression. (**F**) Visual cortex (V1) presented some GFP-positive afferences and the neurons located in the subicullum (S) and postsubicullum (Post) show GFP expression. (**G**) Some GFP-positive afferences onto the oriens layer at the CA3 field of the hippocampus. (**H**) The preoptic area (PO) presented several neurons showing GFP expression. Scale bar = 100 µm.

Extensive analysis showed that transduction was achieved in a variety of nuclei distributed along the brainstem, midbrain and forebrain, as well as in fiber tracts mostly associated with sensorial input. Remarkably, cerebellum presented also strong GFP signal in fibers across the white matter and terminals entering into the granular layer that may be the inputs of mossy fibers (**Figure 19A**). Some scarce cells in the granular and molecular layers, but not Purkinje cells, presented also GFP-positive signal. Along the brainstem, marked GFP expression was observed in most of the neurons at the parabrachial nucleus (**Figure 19B**), locus coeruleus (**Figure 19C**), and several motor nuclei mainly the facial (VII) nuclei (**Figure 19D**), and in minor percentage at the hypoglossal (XII) and vagus (X) motor nuclei. Some neurons were found strongly transduced also in the inferior olive, reticular (**Figure 19D**), solitary, cochlear and prepositus nuclei. Among fibers, we found marked transgene expression in the rubrospinal, trigeminal and spinocerebellar and optic tracts. Along midbrain and forebrain structures, we found strong GFP signal in the pontine reticular area and in the inferior and superior collicula (**Figure 19E**). Dorsally to these structures, in the

cortical area, some GFP-positive neurons in the subicullum and postsubiculum were detected (**Figure 19F**) but rarely along other cortical layers. No remarkable signal was observed in the hippocampus except some afferences into the oriens layer of the CA3 field (**Figure 19G**). More rostrally, strong labeling in the preoptic area (**Figure 19H**) and several scarce GFP-positive neurons in the geniculate nuclei within the thalamus, the hypothalamus, caudate-putamen and ventral pallidum were distinguished. Finally, we also observed some cells transduced at the olfactory bulb, which might be mitral cells because they are neuron-like but they are not stained by NeuN (Mullen et al. (1992)) (**Figure 20A**), and also some transduction of the meninges (not shown).

Most of the cells transduced in the brain exhibit a neuron-like shape, and we confirmed that they were neurons by NeuN colocalization (**Figure 20C**). However, several astrocytes (GFAP positive cells) were detected in some areas (**Figure 20D**). In the brainstem GFP and GFAP signals did not colocalize, suggesting that GFP signal in the brainstem comes from neuronal axons (**Figure 20B**). In addition, several transduced oligodendrocytes (APC positive cells) were detected in some areas (**Figure 20E**). Thus, in brain, the intrathecal administration of AAVrh10 transduces mainly neurons, but it is capable to transduce astrocytes and also oligodendrocytes.

Since the genetic background of the MPS VII mice is C57BL/6, we repeated this tropism experiment using wild type C57BL/6 mice. The results obtained were very similar, except for one feature: in the cortex of C57BL/6 mice we observed GFP expression in brain blood vessels, as it is shown by collagen IV co-labeling (**Figure 20F**). This feature had not been observed in the ICR mouse strain. Although we cannot discard other hypotheses, the strain of the mouse may have a role in this different pattern of transduction.

Figure 20: Cell type characterization in brain after intrathecal AAVrh10 administration. Direct GFP signal in green; cell-type specific marker in red. Scale bars: 70 μm. Insets = 2X magnification. (**A**) NeuN staining in the olfactory bulb, where GFP-positive neurons are NeuN-negative (mitral cells). (**B**) GFAP staining in the brainstem, suggesting GFP is expressed in neuronal axons. (**C**) NeuN staining in cortex, labeling neurons. (**D**) GFAP and (**E**) APC staining in olfactory bulb, labeling astrocytes and oligodendrocytes respectively. (**F**) Collagen IV staining in cortex of C57BL/6 mice, labeling blood vessels.

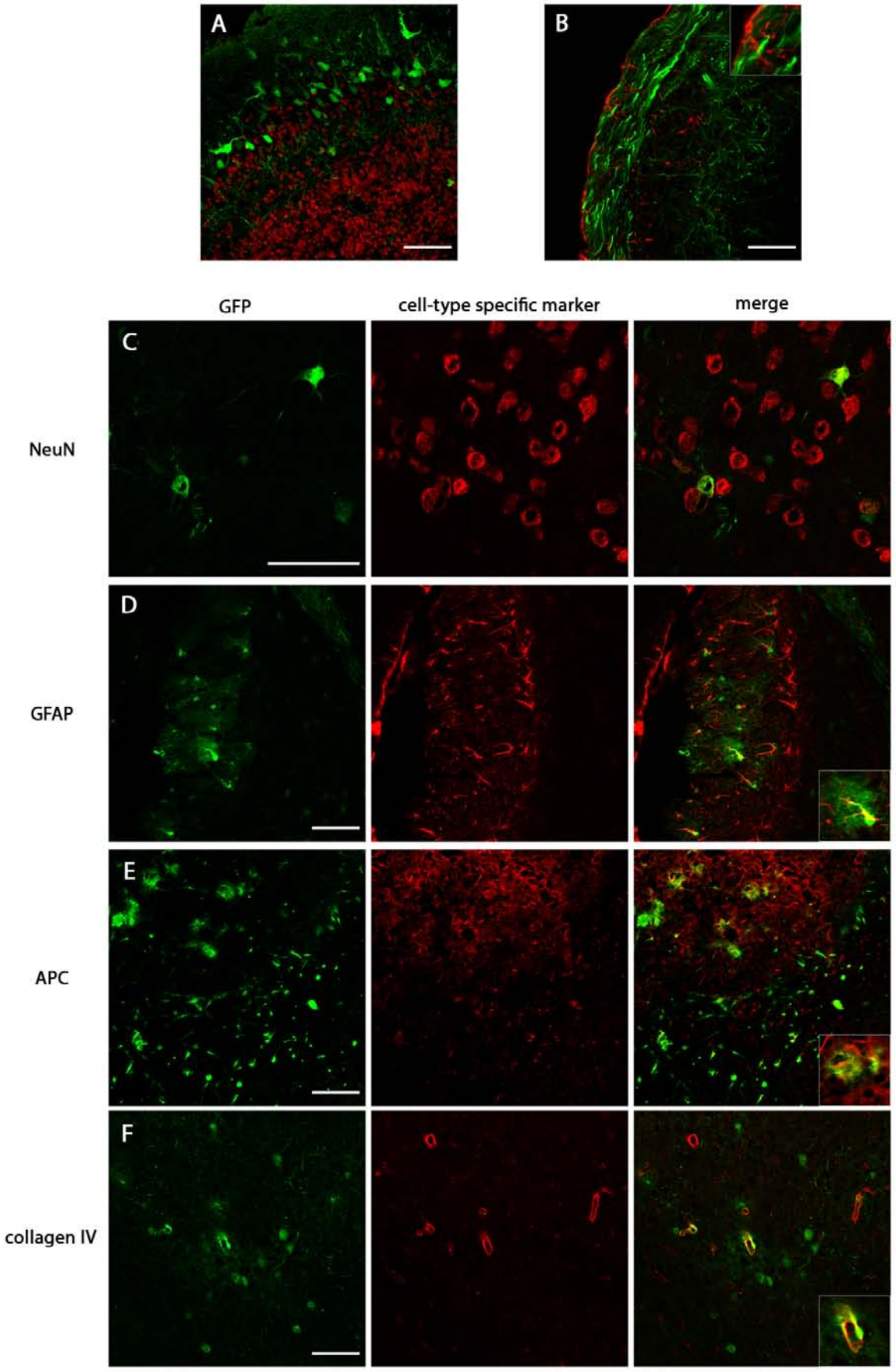
A
B
GFP
cell-type specific marker
merge
C
NeuN
D
GFAP
E
APC
F
collagen IV

1.4. CHOICE OF AAV SEROTYPE AND ADMINISTRATION ROUTE

The aim of this part of the work was to choose the viral vector and the administration route to be used in the gene therapy approach for MPS VII. The results obtained with the intravenous administration of 1.94×10^{12} vg per mouse of either AAV9 or AAVrh10 lead us to think that AAV9 could be the better choice, since this serotype appeared to be more efficient than AAVrh10 in transducing liver and brain. However, the intrathecal injection of 10^{11} vg per mouse of AAVrh10 also demonstrated its efficiency in reaching brain and liver, in addition to its previously described tropism for sensory and motor neurons (Homs et al. (2014)). Therefore, to achieve an efficient transduction of brain and liver, the dose of vector used for intrathecal AAVrh10 administration was 20 times lower than for intravenous AAV9 administration. This significant lower dose, and the evidence that AAVrh10 raises less neutralizing antibodies than AAV9 in mice, lead us to choose the intrathecal AAVrh10 administration for the gene therapy approach for MPS VII.

2. GENE THERAPY TO TREAT MPS VII MICE: INTRATHECAL INJECTION OF AAVrh10-GUSB

MPS VII mice lack β-glucuronidase activity which leads to alterations in the nervous system and in peripheral tissues. Previous results from this work show that intrathecal injection of AAVrh10 is able to transduce cells in the CNS, PNS, and also to cross the BBB to the periphery and transduce cells in the liver. Thus, AAVrh10 could be a good candidate for a gene therapy approach in MPS VII mice. Using GUSB as the transgene, the gene coding for β-glucuronidase, we attempt to restore the enzymatic activity in the nervous system and peripheral tissues, and to improve the disease symptoms and slow disease progression.

This part of the work is divided in two sections:

2.1. Intrathecal AAVrh10-GUSB in MPS VII mice. Pilot study

2.2. Intrathecal AAVrh10-GUSB in MPS VII mice. Survival, biochemical, histological and behavioral effects of short- and long-term treatment

2.1. INTRATHECAL AAVrh10-GUSB IN MPS VII MICE. PILOT STUDY

2.1.1. Experimental design

A pilot study was designed to establish the best conditions for the gene therapy approach concerning the age of the mice at the beginning of the treatment, the dose of AAVrh10-GUSB to inject intrathecally, and the duration of the treatment.

Two experimental designs were performed for the pilot studies (PS) (**Figure 21**):

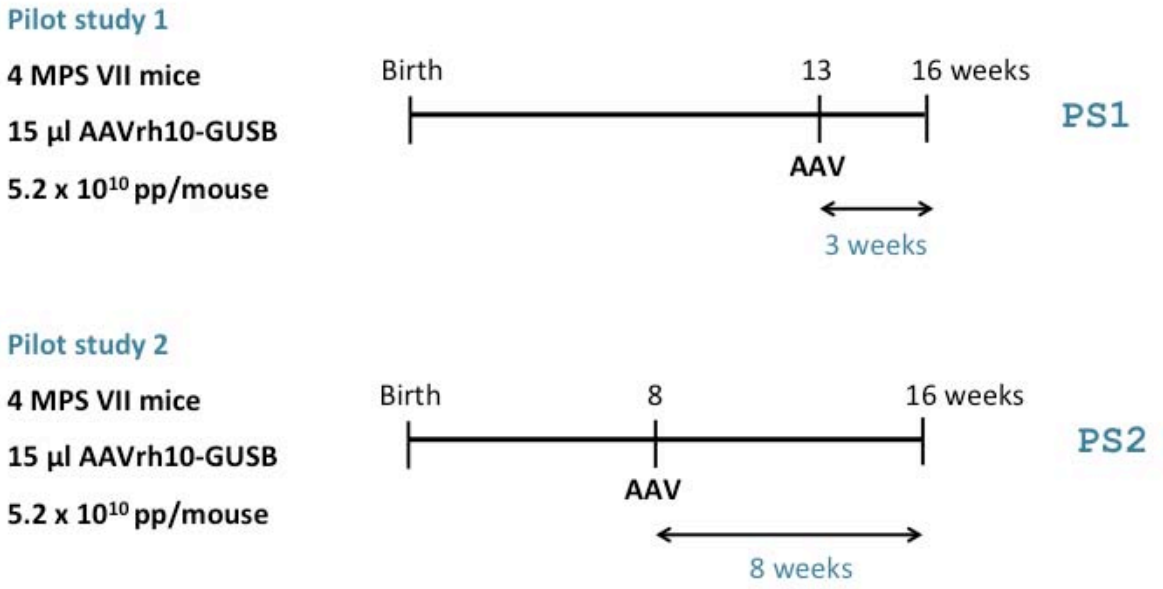

Figure 21: Data and timeline of the pilot studies in MPS VII mice.

PS1: 4 MPS VII mice, 13 weeks old, were injected IT with AAVrh10-GUSB, at a dose of 5.2 x 10^{10} vg per mouse in 15 µl. Sacrificed three weeks later, at 16 weeks of age, approximately 4 months old.

PS2: 4 MPS VII mice, 8 weeks old, were injected IT with AAVrh10-GUSB, at a dose of 5.2 x 10^{10} vg per mouse in 15 µl. Sacrificed 8 weeks later, at 16 weeks of age, approximately 4 months old. One mouse of 3.5 months of age was used for fixed tissue analysis.

2.1.2. Biochemical analysis

2.1.2.1. In toto β-glucuronidase staining

In order to have a general illustration of the β-glucuronidase activity provided by the AAVrh10-GUSB IT injection, one of the treated MPS VII mice in PE2 was sacrificed after 7 weeks, tissues were fixed, and in toto β-gluc activity staining was performed. **Figure 22** shows 100 μm vibratome slices of brain, lumbar SC and lumbar DRG exhibiting red deposits, which reveal the β-gluc activity. In brain, an abundant and widespread β-gluc activity is evident in different areas, particularly in cortex, septal nuclei (part of striatum, in basal ganglia) and preoptic area (part of hypothalamus), while caudatoputamen structures (part of striatum, in basal ganglia) shows low enzymatic activity. Spinal cord also displays broad β-gluc activity, mainly in the areas where somata of motor neurons are located, and also in the dorsal and ventral white matter, where sensory and motor nerve roots are, respectively. β-Gluc activity in lumbar DRG is restricted to several large cells that are likely to be sensory neurons transduced by the AAV vector, which is consistent with previous observations in wild type mice treated with AAVrh10-GFP (Homs et al. (2014)). In contrast to these images, WT tissue displays a faint background staining, which indicates much lower β-gluc activity levels (not shown).

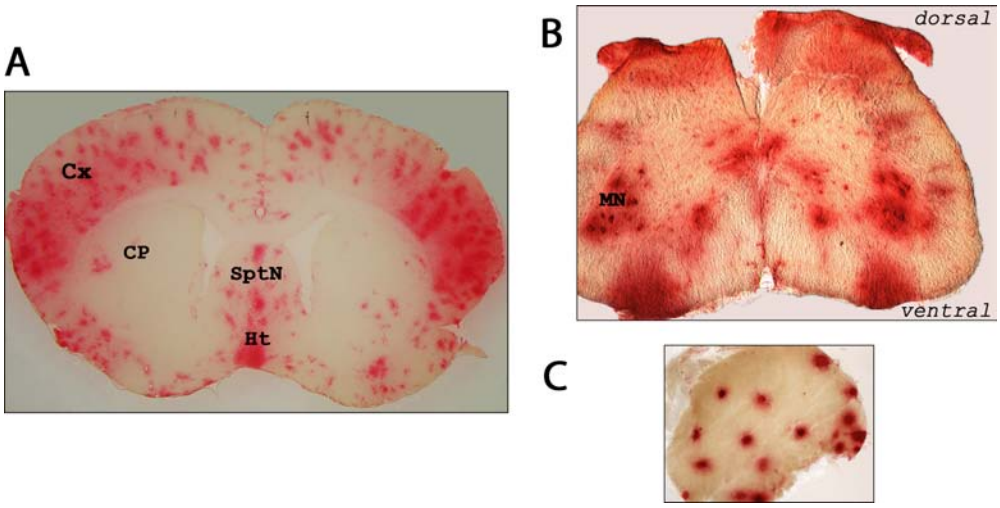

Figure 22: In toto β-glucuronidase staining in samples of a MPS VII mouse injected intrathecally with 5.2 x 10^{10} vg of AAVrh10-GUSB in 15 μl. (**A**) Brain coronal section. *Cx,* cortex; *SptN*, septal nuclei; *PO*, preoptic area; *CP*, caudatoputamen; (**B**) Lumbar spinal cord section. *MN*, motor neurons. (**C**) Lumbar dorsal root ganglion.

2.1.2.2. β-Glucuronidase activity

β-Glucuronidase activity was analyzed in frozen tissue samples of CNS, PNS, liver and serum of the MPS VII mice injected in the preliminary experiments PE1 and PE2. Brains were dissected in seven 2-mm coronal slices as shown in **Figure 23**. Spinal cord and DRG were separated in four regions: cervical, upper thoracic, lower thoracic and lumbar.

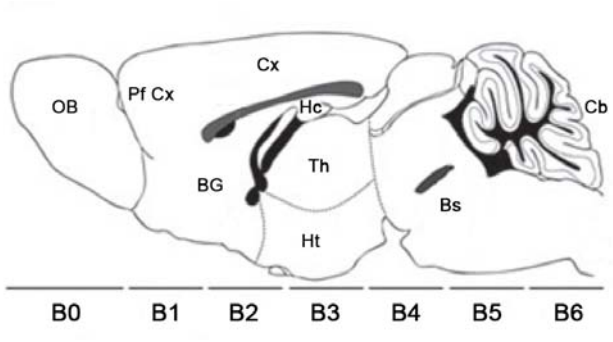

Figure 23: Brain regions and dissection. Seven coronal 2-mm slices, labeled B0 to B6.

Samples were homogenized and β-gluc activity was assayed by the addition of a specific substrate (4-methylumbelliferyl-β-D-glucuronide), and the product of the reaction can be quantified by fluorescence. **Figure 24** shows the scatter plots of the β-gluc activity of each mouse, represented in relative light units (RLU) normalized by the total protein content in each sample, or by volume in the serum samples. β-Gluc activities of the MPS VII injected mice are compared to HTZ mice of the same age. HTZ mice present β-gluc activity levels approximately one-half of those of WT mice, which is enough for the physiological action because they do not display MPS VII phenotype (Birkenmeier et al. (1989)).

Figure 24: β-Glucuronidase activity in pilot study 1 (A to E) and pilot study 2 (F to J). Data from a mouse that was probably not correctly injected are circled. **(A and F)** Brain dissected in coronal slices. **(B and G)** Spinal cord. **(C and H)** DRG and sciatic nerve. **(D and I)** Liver. **(E and J)** Serum. Tissue samples normalized by total protein content. Serum samples normalized by volume. RLU: Relative light units. Sample sizes depicted on the graphs, where — denotes the mean. Abbreviations: *cv*, cervical; *up-th*, upper thoracic; *low-th*, lower thoracic; *lmb*, lumbar; *sciatic*, sciatic nerve.

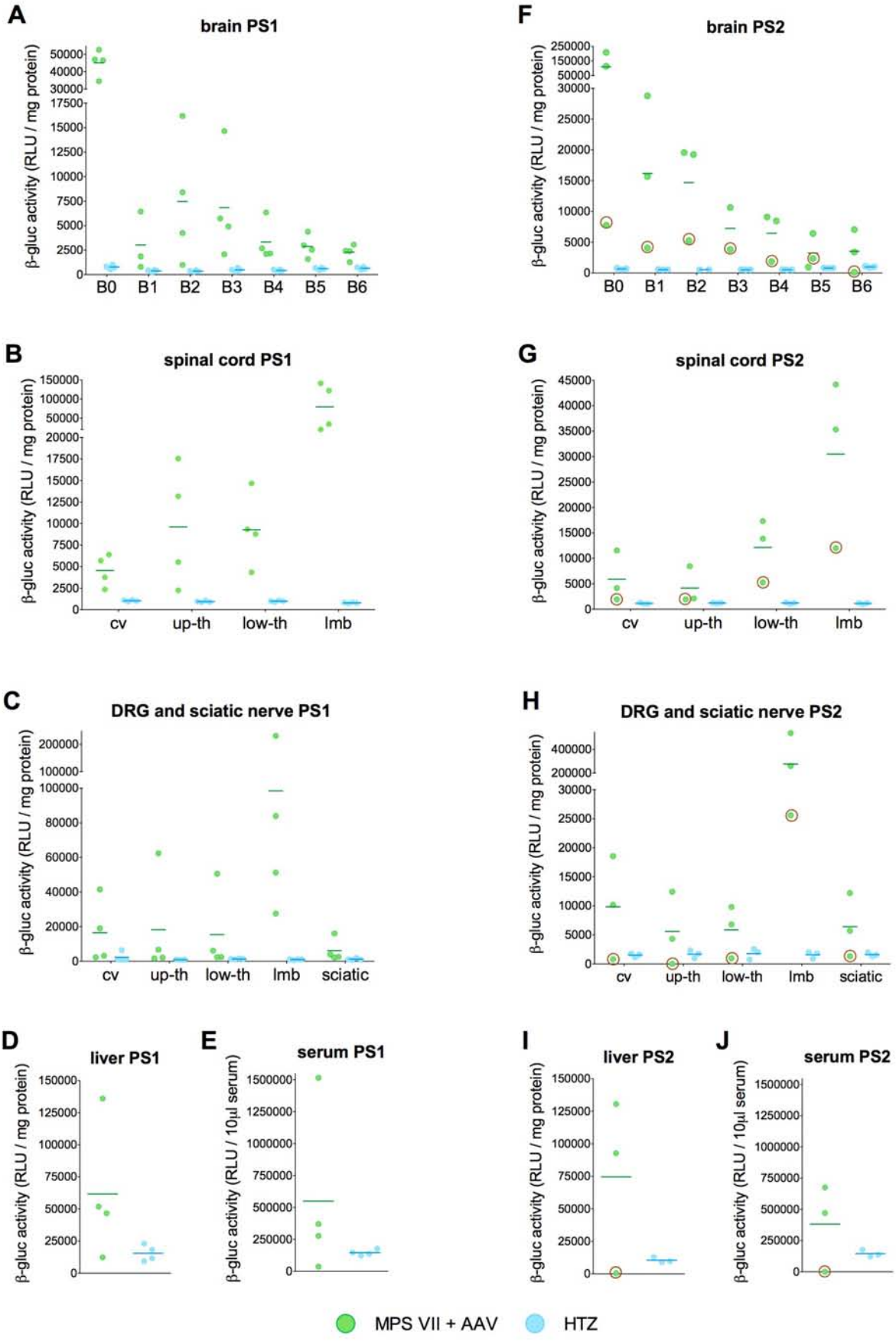
A
brain PS1
β-gluc activity (RLU / mg protein)
B0 B1 B2 B3 B4 B5 B6
F
brain PS2
β-gluc activity (RLU / mg protein)
B0 B1 B2 B3 B4 B5 B6
B
spinal cord PS1
β-gluc activity (RLU / mg protein)
cv up-th low-th lmb
G
spinal cord PS2
β-gluc activity (RLU / mg protein)
cv up-th low-th lmb
C
DRG and sciatic nerve PS1
β-gluc activity (RLU / mg protein)
cv up-th low-th lmb sciatic
H
DRG and sciatic nerve PS2
β-gluc activity (RLU / mg protein)
cv up-th low-th lmb sciatic
D
liver PS1
β-gluc activity (RLU / mg protein)
E
serum PS1
β-gluc activity (RLU / 10µl serum)
I
liver PS2
β-gluc activity (RLU / mg protein)
J
serum PS2
β-gluc activity (RLU / 10µl serum)
MPS VII + AAV
HTZ

In both experiments, animals show high levels of β-gluc activity compared to HTZ mice. Although the mean activity levels are higher than HTZ in all the areas analyzed, there is great dispersion of the data in each area, with important differences between mice and several data below the HTZ mean activity.

As it was expected, β-glucuronidase activity in lumbar DRG and lumbar SC is higher than in other DRG and SC areas, as they are closer to the AAV injection site and transduction is better. It is also noteworthy that the β-gluc activity in "brain 0" slice, which corresponds to the olfactory bulb, is extremely high when compared to other brain areas. This could be due to the anatomy of the olfactory bulb: a small structure with nearly its whole external surface bathed by CSF. This fact could enhance the transduction after intrathecal AAV administration. Nevertheless, we cannot discard the presence of some specific receptor for AAVrh10 that could be highly expressed in the olfactory bulb.

2.1.2.3. β-Hexosaminidase activity

In the MPS VII mouse, β-hexosaminidase (β-hex) activity is increased, as other lysosomal hydrolases, as a compensatory response to the lack of β-glucuronidase. Mouse samples from experiments PS1 and PS2 were tested for β-hex activity and compared to HTZ and to MPS VII mice of the same age. Results are represented in **Figure 25** as ratios relative to HTZ, and statistical analysis was performed by one-way ANOVA followed by Tukey post hoc test.

Figure 25: β-Hexosaminidase activity relative to HTZ in (**A**) brain slices (**B**) spinal cord regions (**C**) dorsal root ganglia regions and sciatic nerve, and (**D**) liver. Statistics: One-way ANOVA $p < 0.001$ in all the cases (not depicted) and Tukey post-hoc: * vs. HTZ; $^{\#}$ vs. MPS VII; $^{\$}$ between AAV-treated groups. Samples sizes: n = 4 MPS VII; n = 4 MPS VII + AAV PS1; n = 3 MPS VII + AAV PS2; n = 7 HTZ.

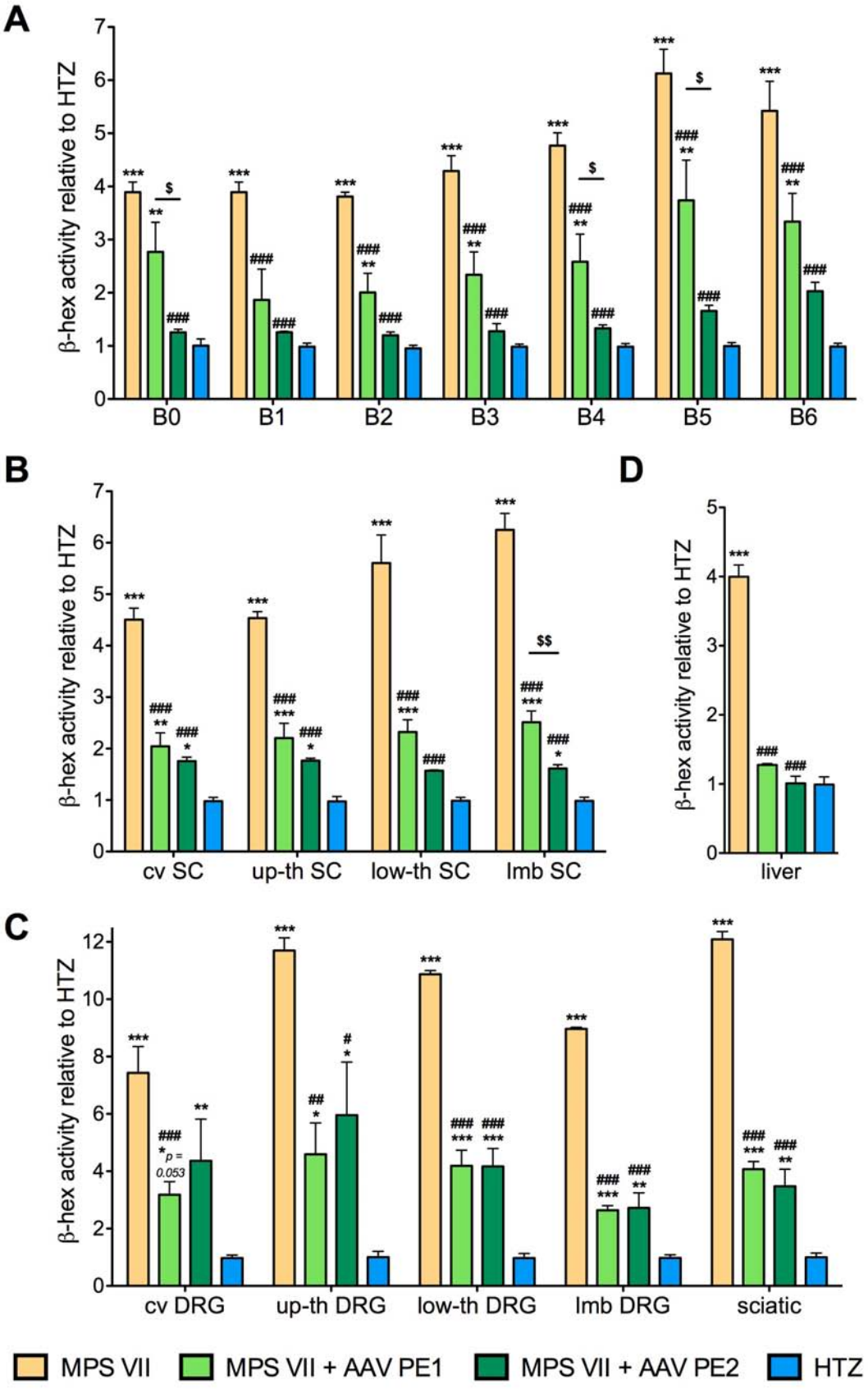
A
β-hex activity relative to HTZ
B0
B1
B2
B3
B4
B5
B6
B
cv SC
up-th SC
low-th SC
lmb SC
D
liver
C
cv DRG
up-th DRG
low-th DRG
lmb DRG
sciatic
p = 0.053
MPS VII
MPS VII + AAV PE1
MPS VII + AAV PE2
HTZ

In all the areas analyzed, MPS VII mice samples present higher β-hex activity than HTZ mice. The treatment with AAVrh10-GUSB is able to lower β-hex activity in both experiments, although in different degree depending on the area and the experiment. It is important to notice that β-hex activity in liver is normalized to HTZ levels, which suggests a biochemical correction in livers of MPS VII treated mice.

As stated before, PS1 mice were treated when they were older than PS2 mice, and the treatment duration was shorter. Since lysosomal storage is accumulating progressively along the life of MPS VII mice and patients, the later the treatment starts, the more storage will need to be metabolized and it will take longer time. Consequently, secondary activated lysosomal enzymes will take longer to reach normal activity.

It is also noteworthy that, in DRG and sciatic nerve samples, as well as in the majority of spinal cord areas, the treatment is able to reduce but not to normalize β-hex activity to HTZ levels. This can be due to the high levels of β-hex activity present in MPS VII DRG and sciatic nerve, which are the highest from all samples analyzed, when compared to HTZ. In spinal cord, despite MPS VII β-hex levels are not as high as in DRG, the correction is not complete in AAV-treated mice, although it is closer to HTZ.

Finally, it is significant that β-hex activity from the three PS2 AAV-treated mice is similar in most of the areas analyzed (brain, spinal cord and liver) with small SEM in all the cases. Those data include a mouse that was probably not correctly treated, which had the lowest β-gluc activity levels in all areas (circled data in **Figure 25F-J**). Thus, it suggests that, even with very low β-gluc activity, β-hex activity can be considerably reduced.

2.1.3. Biodistribution of the AAV-vector DNA

Considering that β-glucuronidase expressed by the transgene can be secreted from the transduced cells, we wanted to determine whether tissues showing β-gluc expression had been transduced by the AAVrh10-GUSB vector or had captured the lysosomal enzyme through the mannose-6-phosphate receptor from cells transduced in other areas. Samples from mice of experiment PS1, injected intrathecally with 5.34 x 10^{10} vg per mouse, were used to quantify the AAVrh10-GUSB vector DNA by qPCR. In order to determine the number of vector copies per cell, vector DNA quantification was compared to cyclophilin quantification, a gene with only one copy per cell. Although the vector DNA quantity was close to the lower quantification limit of the standard curve, all the areas analyzed were apt for quantification, except for sciatic nerve samples, and results are shown in **Figure 26**.

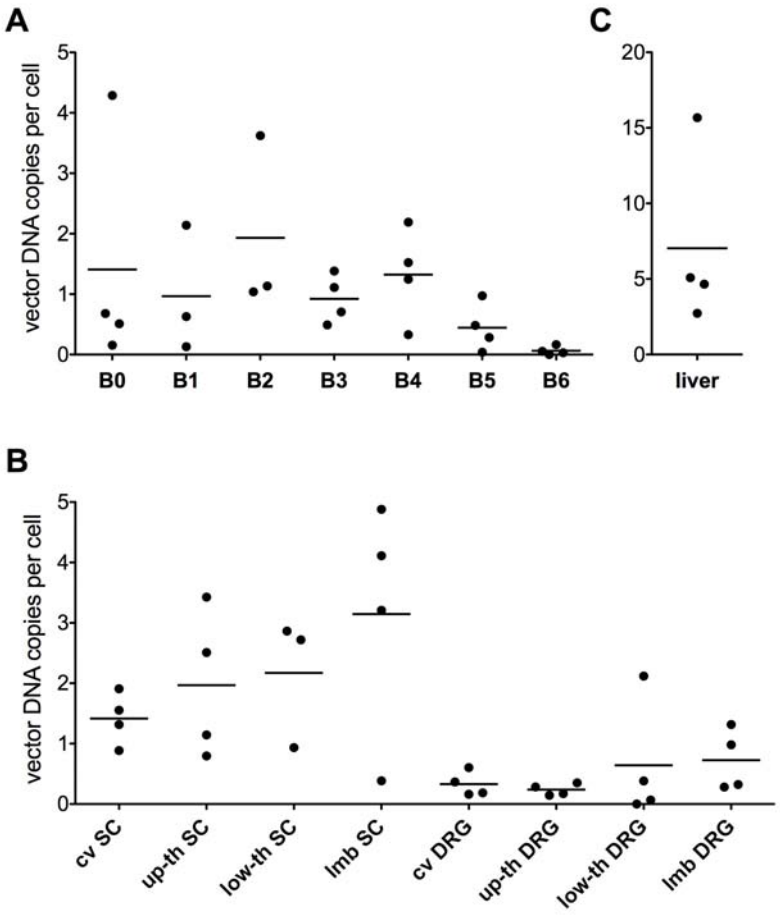

Figure 26: AAV-vector DNA quantification by qPCR in (**A**) brain slices, (**B**) spinal cord and DRG areas and (**C**) liver. Sample sizes depicted on the graphs, where — denotes the mean.

In the CNS and PNS samples, vector DNA quantification is in a range of 0 to 5 vector copies per cell, and there are important differences between mice in most of the areas. As it was expected, AAV-vector DNA is also found in liver samples because of vector leakage from the CSF to the bloodstream. Surprisingly, the vector copies per cell in liver are higher than in any other area analyzed. This fact could be due to differences in the DNA extraction among different tissues. Despite we used Hirt protocol to favor low molecular weight DNA extraction, we cannot discard differences in the ratio of high vs. low molecular weight DNA in different tissues, which could alter the relative amounts of vector DNA vs. cyclophilin DNA.

As a complementary preliminary experiment, 4 WT mice were injected intrathecally with a lower dose of AAVrh10-GUSB, 1.75 x 10^{10} vg/mouse. Mice were sacrificed after 3 weeks and the quantity of AAV-vector DNA was analyzed by qPCR. The vector DNA was detected in all the samples analyzed, although it could not be quantified because it was below the quantification limit of the standard curve in all the cases (data not shown). Thus, the lower dose of AAVrh10-GUSB was also able to reach all the areas analyzed.

With these preliminary experiments we demonstrated that with an intrathecal dose of 5.2 x 10^{10} vg/mouse of AAVrh10-GUSB a number of vector copies per cell are detected in CNS, PNS and liver. These vector copies give rise to high β-glucuronidase activity in all the areas analyzed and lead to partial or total β-hexosaminidase activity correction when compared to MPS VII and to HTZ mice. This biochemical correction appears to be higher when mice are injected at a younger age and with a longer duration of the treatment. Moreover, we showed that a lower dose of 1.75 x 10^{10} vg/mouse of AAVrh10-GUSB is also able to transduce cells in all the areas analyzed. Since β-gluc levels of high-dose transduced animals were much higher than those of WT or HTZ mice, we considered that treating MPS VII mice with the low dose could be sufficient to expect β-glucuronidase activity to be therapeutically efficient, thus increasing biosafety by reducing the virus load. Yet, starting the treatment at 8 weeks of age and extending it for 8 weeks or more could be a suitable therapeutic approach to evaluate the efficiency of the gene therapy treatment in MPS VII mice.

2.2. INTRATHECAL AAVrh10-GUSB IN MPS VII MICE. BIOCHEMICAL, HISTOLOGICAL, BEHAVIORAL AND SURVIVAL EFFECTS OF SHORT- AND LONG-TERM TREATMENT

2.2.1. Experimental design

After the pilot study, a larger group of MPS VII mice were treated in order to assess the biochemical, histological and behavioral effects of the intrathecal injection of AAVrh10-GUSB at two treatment time points. The key features of the experimental design are described in in **Table 3** and the timeline is shown in **Figure 27.**

Table 3: Experimental design

Treatment was administered to **8-week-old mice** by **intrathecal injection**.
The volume of vector injected was **5 µl**, corresponding to 12% of total CSF volume.
The dose of AAVrh10-GUSB injected was **1.75 x 10^{10} vg/mouse**.
Control mice were injected with 5 µl of an empty AAVrh10 vector.
Short-term time point: 6 weeks after AAV injection, when mice were **3.5 months old.**
Long-term time point: 16 weeks after AAV injection, when mice were **6 months old.**
At each time point, **4 different groups** were determined: **MPS VII:** MPS VII homozygote mice as disease controls. **MPS VII + AAV:** MPS VII homozygote mice injected with AAVrh10-GUSB. **HTZ:** MPS VII heterozygote mice, without phenotype, as healthy controls. **WT:** C57BL/6 wild type mice as healthy controls.
Mice were kept in a SPF mouse facility until the treatment end point. Then, behavioral tests were carried out in a conventional laboratory room during three days. Mice were sacrificed after the last behavioral test and tissue samples were collected.
The number of injected mice per group ranged from 8 to 12. However, several MPS VII mice spontaneously died during the follow-up time due to the disease.

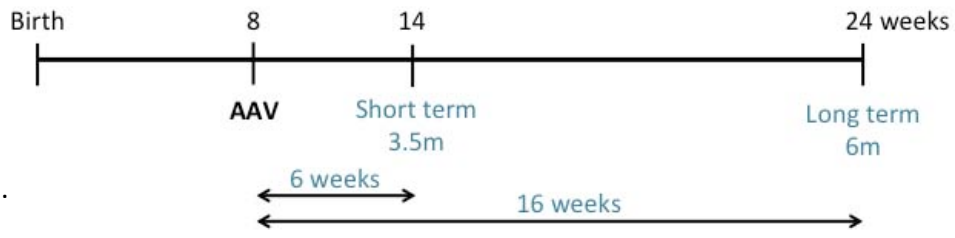

Figure 27: Experimental design timeline.

In parallel to this experiment, a group of MPS VII mice were treated with AAVrh10-GUSB and were kept in the animal facility until they spontaneously died, in order to evaluate the effect of the treatment in the survival of MPS VII mice (see section 2.2.6).

2.2.2. Organ weight

It is described that MPS VII patients present hepatomegaly and splenomegaly. Thus, we wanted to evaluate these characteristics in our MPS VII mice and, if confirmed, to test the efficacy of the AAV treatment to revert them to WT parameters. With this aim, at the moment of mouse euthanasia, liver and spleen were dissected, blood was drained and each organ was weighed. The percentages of organ weight vs. body weight were calculated and compared between experimental groups and mouse ages.

We found that spleen weight does not present any differences attributed to the experimental group (F (3,48) = 1.8, $p > 0.05$) or to the age (F (1,48) = 2.864, $p > 0.05$).

In contrast, we found differences in liver weight depending on the experimental group (F (3,48) = 6.046, $p = 0.001$) but not on the age of mice (F (1,48) = 0.305, $p > 0.05$). **Figure 28** represents relative liver weight pooling together both ages of each group, since the age does not affect the liver weight. Results show that MPS VII liver weight is higher than WT and HTZ, and that the treatment with AAVrh10-GUSB is able to correct this abnormality, reducing MPS VII liver to WT and HTZ size.

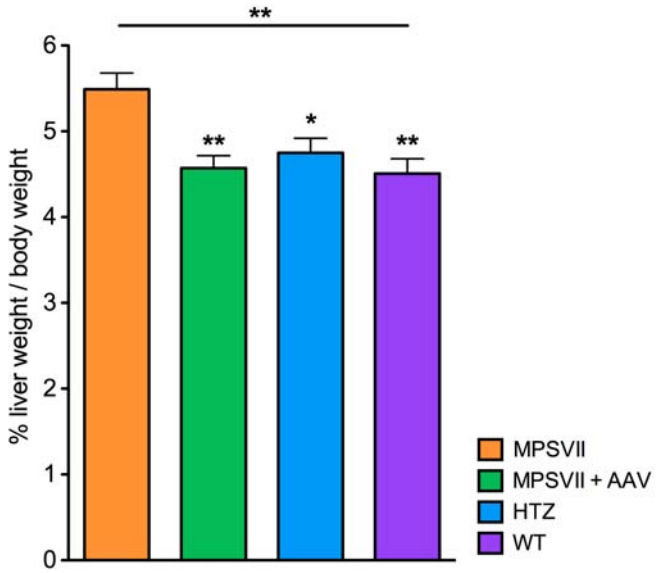

Figure 28: Liver weight, relative to body weight of mice. Each bar represents data from the two experimental time points pooled together. Statistical analysis performed by one-way ANOVA and Tukey post hoc. Sample sizes: n = 13 MPS VII; n = 13 MPS VII + AAV; n = 14 HTZ; n = 16 WT.

2.2.3. Biochemical analysis

2.2.3.1. In toto β-glucuronidase staining

With the aim to have a general overview of the β-glucuronidase activity in MPS VII tissues, we performed in toto β-gluc staining on AAV-treated samples taken 3.5 months after injection. **Figure 29** shows 100-μm slices of brain, spinal cord, dorsal root ganglia and liver, where red deposits reveal the areas with higher β-glucuronidase activity.

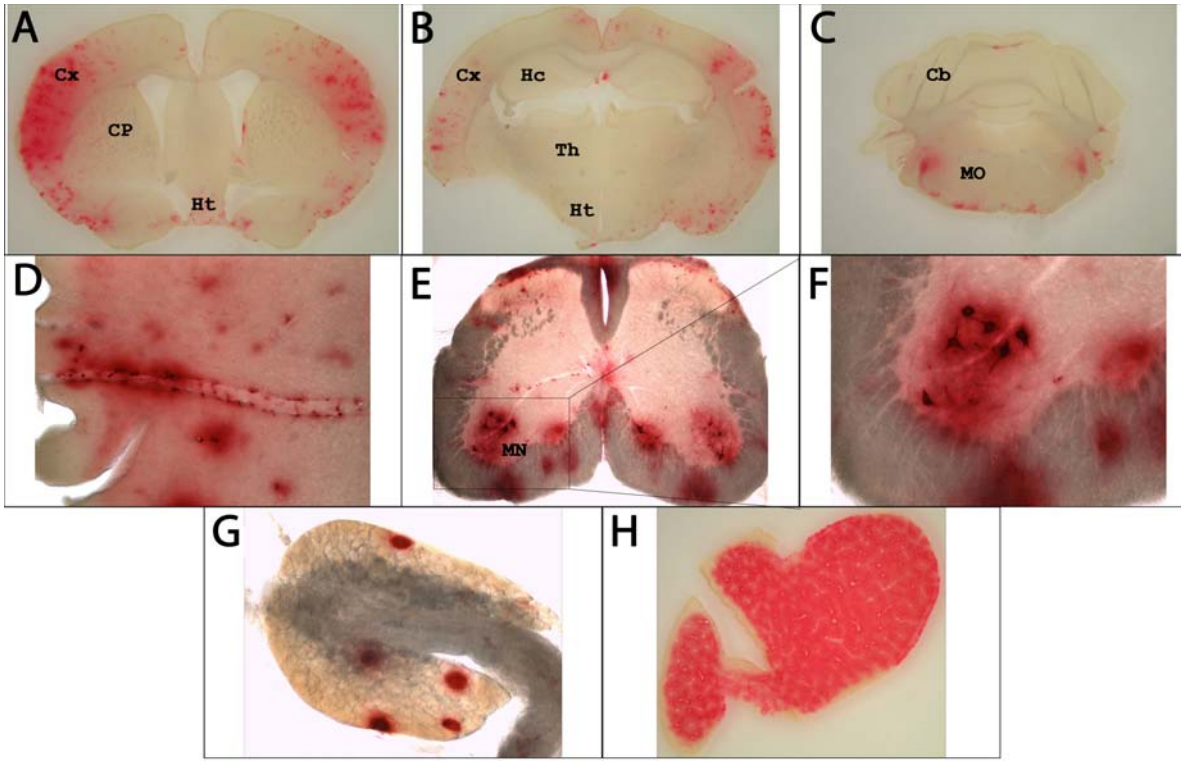

Figure 29: In toto β-Glucuronidase staining in AAV-treated MPS VII mice. (**A-C**) Brain coronal sections showing different anatomical regions: *Cx*, cortex; *CP*, caudatoputamen; *Ht*, hypothalamus; *Hc*, hippocampus; *Th*, thalamus; *Cb*, cerebellum; *MO*, medulla oblongata. (**D**) Magnification of a cortex area displaying high intensity β-gluc staining associated to blood vessels. (**E**) Lumbar spinal cord section exhibiting high intensity staining in motor neurons, *MN*, at higher magnification in (**F**). (**G**) Lumbar dorsal root ganglion. (**H**) Liver section, displaying widespread high intensity β-gluc staining.

Brain coronal slices from three different areas (**Figure 29A-C**) show high β-gluc activity mainly in cortex. Other areas, such as hypothalamus, cerebellum and medulla oblongata (part of the brainstem), also present β-gluc staining, although it is less

widespread than in cortex. A magnification of the cortex area (**Figure 29D**) reveals that several of the high intensity β-gluc spots are located near blood vessels, which are identified by morphologic characteristics. This observation correlates with the data of GFP-transduced mice from previous experiments, where positive cells co-localized with the blood vessel marker collagen IV (see Figure 20F). **Figure 29E-F** show that spinal cord presents the highest β-gluc activity in the ventral area, with several cells displaying intense β-gluc staining. These cells are identified as motor neurons by their morphology and localization. Dorsal and ventral SC roots also present β-gluc activity, as well as some areas in the white matter parenchyma that could also correspond to blood vessels. Dorsal root ganglia also present β-gluc activity, with high intensity staining in several cells, consistent with AAV-transduced sensory neurons (**Figure 29G**), correlating with previous data using GFP (Homs et al. (2014)). Finally, in **Figure 29H** it is shown that liver presents very high β-gluc activity, with a homogeneous and widespread signal in the whole slice, suggesting that a large amount of liver cells were transduced by AAVrh10-GUSB, as it was expected.

Since the dose of AAVrh10-GUSB (1.75×10^{10} vg/mouse) was three times lower than in the pilot study, tissue transduction and therefore β-gluc activity by in toto staining is significantly lower than in previous results (see Figure 22), but still higher than in HTZ or WT mice samples that display a faint background staining (not shown).

2.2.3.2. β-Glucuronidase activity

β-Glucuronidase activity assay in frozen tissue samples was performed in CNS and PNS samples, as well as in serum, liver, heart and lumbar intervertebral discs of HTZ, WT and AAV-treated MPS VII mice, at both treatment time points. In this case, brains were dissected in 8 structural areas, as it is shown in **Figure 23**: olfactory bulb (*OB*), prefrontal cortex (*Pf Cx*), cortex (*Cx*), hippocampus (*Hc*), thalamus and basal ganglia (*Th +BG*), hypothalamus (*Ht*), cerebellum (*Cb*) and brainstem (*Bs*).

When analyzing the data, and before comparing between groups, it was evident that β-gluc activity of AAV-treated MPS VII mice presented high variability between mice

in all the areas analyzed. In order to check if there could be any effect of the gender of the mice in the β-gluc activity after intrathecal AAVrh10-GUSB delivery, we compared data from both sexes by two-tailed *t*-tests. Representative organs and areas depicted in **Figure 30**.

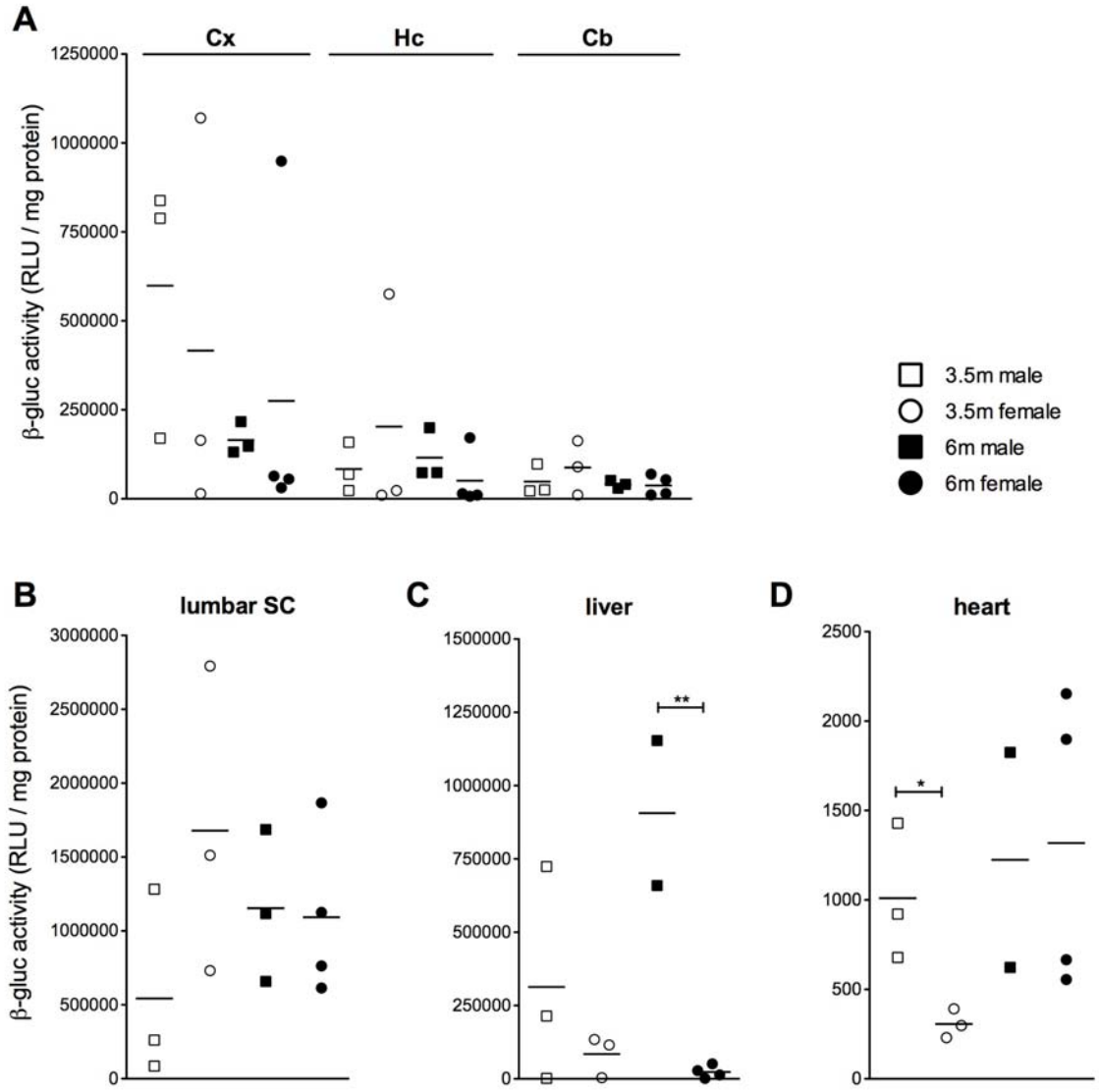

Figure 30: β-Glucuronidase activity of AAV-treated MPS VII between genders. Representative areas. Sample sizes depicted on the graphs, where — denotes the mean. Statistics: independent *t*-tests between genders for each time point.

In general, in brain, spinal cord and DRG we cannot attribute the variability in β-gluc expression to the mouse gender (**Figure 30A-B** and data not shown). In contrast, in somatic organs the statistical analysis revealed that β-gluc expression is higher in

males than in females in two cases: heart of 3.5-month-old mice and liver of 6-month-old mice (**Figure 30C-D**). However, the sample size for each group is very small (n = 2 to n = 4), and, furthermore, the differences in each organ are not consistent between the two time points. Therefore, even with the reported statistics, we cannot conclude that the gender of the mice affects somatic organ β-glucuronidase activity after intrathecal AAVrh10-GUSB administration.

As stated before, the variance of the data from the AAV-treated MPS VII mice group is highly different than HTZ and WT groups in all the areas analyzed (checked by Levene test). Therefore, since data do not satisfy the parametric assumptions, non-parametric statistical tests were performed to analyze differences between groups. First, we performed Kruskal-Wallis tests to analyze all the groups together and check whether there are overall differences. After this omnibus test, successive Mann-Withney U tests are used to do pairwise comparisons and determine specifically which of the groups are different.

Comparisons were performed separately for each treatment time point, because the experimental timeline did not allow analyzing all the samples at the same time, and pooling together raw data from different analysis could lead to errors due to experimental variability in the analysis procedure. However, β-gluc analysis was repeated for some representative areas and no differences were found between 3.5-month-old and 6-month-old AAV-injected mice (data not shown). Non-treated MPS VII mice were not analyzed for β-gluc activity since it is close to zero and negligible when compared to WT of HTZ mice (Sly et al. (2001)).

Omnibus statistical analysis of the β-glucuronidase activity data for each tissue/area and for each experimental time point (**Table 4**) shows overall differences among the three experimental groups (MPS VII + AAV, HTZ and WT) in many of the analyzed areas.

Table 4: Kruskal Wallis statistical test for β-Glucuronidase activity of AAV-treated MPS VII, HTZ and WT mice. Sample sizes for each group range from *n* = 6 to *n* = 8.

PERIPHERAL TISSUES	3.5m	6m
serum	*	*ns*
liver	*ns*	*ns*
heart	*ns*	*ns*
intervertebral discs	*ns*	*ns*

BRAIN STRUCTURES	3.5m	6m
olfactory bulb (OB)	*	**
prefrontal cortex (Pf Cx)	*ns*	*
cortex (Cx)	*	*ns*
hippocampus (Hc)	*	*ns*
thalamus + basal ganglia (Th + BG)	*ns*	**
hypothalamus (Ht)	*	*ns*
cerebellum (Cb)	*	**
brainstem (Bs)	*	*ns*

SPINAL CORD AND PNS STRUCTURES	3.5m	6m
cervical spinal cord (cv-SC)	**	***
thoracic spinal cord (th-SC)	**	***
lumbar spinal cord (lmb-SC)	**	***
cervical DRG (cv-DRG)	**	**
thoracic DRG (th-DRG)	*	*
lumbar DRG (lmb-DRG)	**	***
sciatic nerve	**	***

* $p < 0.05$
** $p < 0.01$
*** $p < 0.001$
ns, not significant

These differences, in most of the cases, are because β-gluc activity of AAV-injected mice, not only reaches WT levels but it achieves supraphysiologic values. Subsequently, successive Mann-Whitney U tests were performed to dissect pairwise differences, and statistically significant data are reported in **Figures 31**, **32** and **33.**

In general, comparisons between HTZ and WT show that HTZ mice display lower β-gluc activity than WT, although they are not statistically different in all the areas analyzed. β-Gluc activity of HTZ is around or above 50% of WT activity, which correlates with published data (Birkenmeier et al. (1989)).

Figure 31 shows β-gluc activity at each time point of the peripheral organs and structures analyzed: serum, liver, heart and lumbar intervertebral discs. The treatment with AAVrh10-GUSB in MPS VII mice is able to attain β-glucuronidase levels indistinguishable from WT mice at both treatment time points in all the cases.

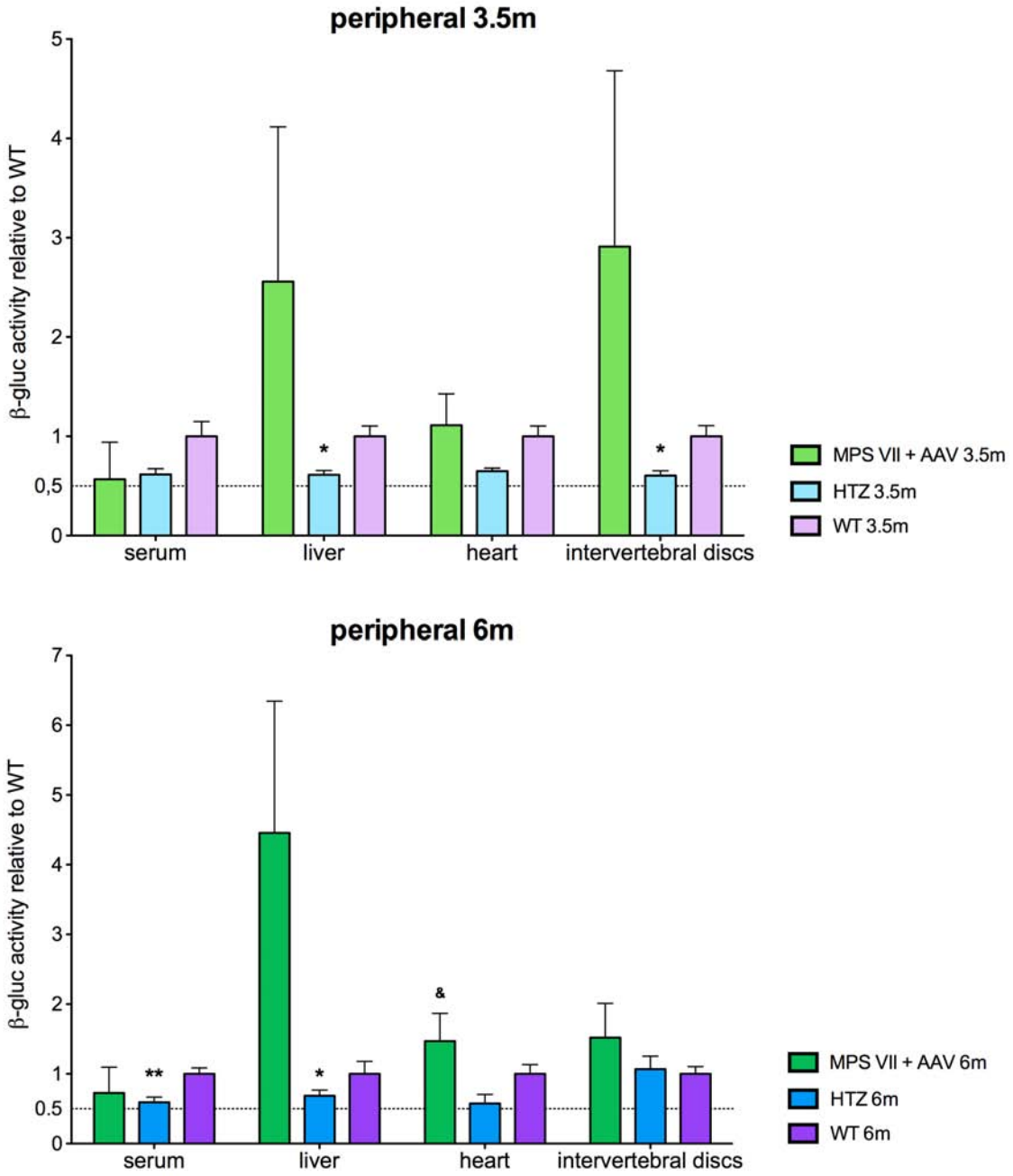

Figure 31: β-Glucuronidase activity in peripheral organs and structures expressed as ratios vs. WT mice. Statistical analysis by pairwise Mann-Whitney U tests. * vs. WT, $^{\&}$ vs. HTZ. Sample sizes from $n = 6$ to $n = 8$.

Figure 32 shows β-gluc activity in the different brain areas analyzed, at both time points.

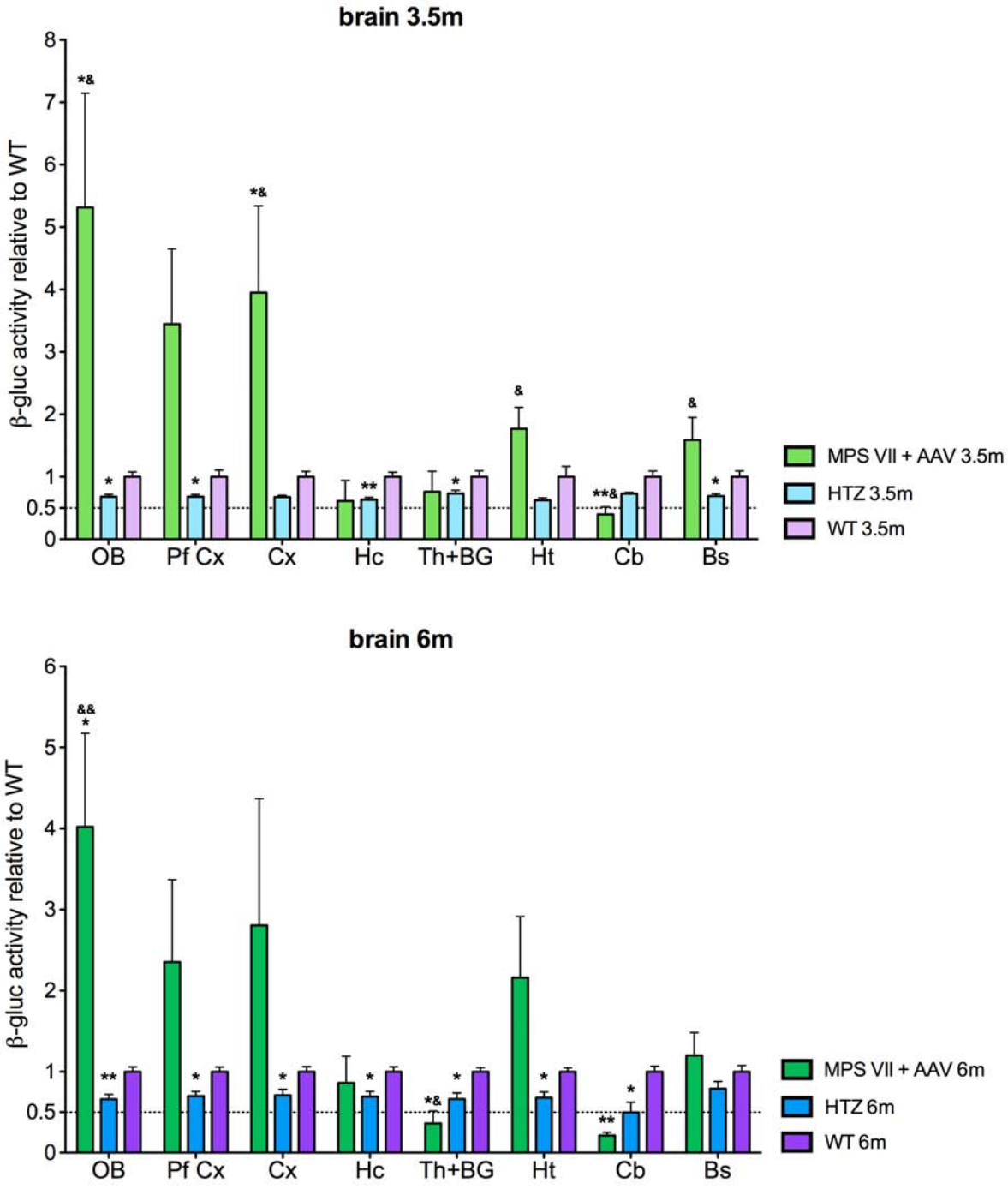

Figure 32: β-Glucuronidase activity in brain structural areas expressed as ratios vs WT mice. Statistical analysis by pairwise Mann-Whitney U tests. * vs. WT, & vs. HTZ. Sample sizes from *n* = 6 to *n* = 8. *OB*, olfactory bulb; *Pf Cx*, prefrontal cortex; *Cx*, cortex; *Hc*, hippocampus; *Th + BG*, thalamus and basal ganglia; *Ht*, hypothalamus, *Cb*, cerebellum; *Bs*, brainstem.

In brain samples, in general, MPS VII treated mice present β-gluc activity levels comparable to those of WT mice, and in some cases statistically higher than HTZ mice, in most areas analyzed and with both treatment durations. Moreover, in olfactory bulbs of AAV-treated mice, β-gluc levels are even higher than in WT mice, as well as in cortex of 3.5-month-old mice. In contrast, and consistent with the in toto staining, in the area that pools thalamus and basal ganglia, although β-gluc activity at 3.5 months is comparable to WT, it is lower than WT and also than HTZ mice at 6 months. In cerebellum statistics also show that AAV-treatment is not able to attain WT levels of β-gluc activity at any time point, but achieves HTZ levels in 3.5-month-old mice. Even though β-gluc activity seems to be lower at 6 months in these two areas of the CNS, this does not indicate that transgene activity is decreasing overtime, since differences between these 2 time-points are not statistically significant (statistics not shown). In conclusion, the intrathecal approach achieved widespread β-glucuronidase expression in all the areas of the brain after AAVrh10-GUSB administration, even reaching supraphysiologic levels in some areas.

When analyzing samples from spinal cord, DRG and sciatic nerves (**Figure 33**), β-gluc activity in AAV-treated MPS VII mice is either comparable or higher than that of WT mice in all the cases. Lumbar SC and DRG are the areas with the more elevated β-gluc activity, which is expected since the AAVrh10-GUSB is injected intrathecally in the lumbar region (Homs et al. (2014)).

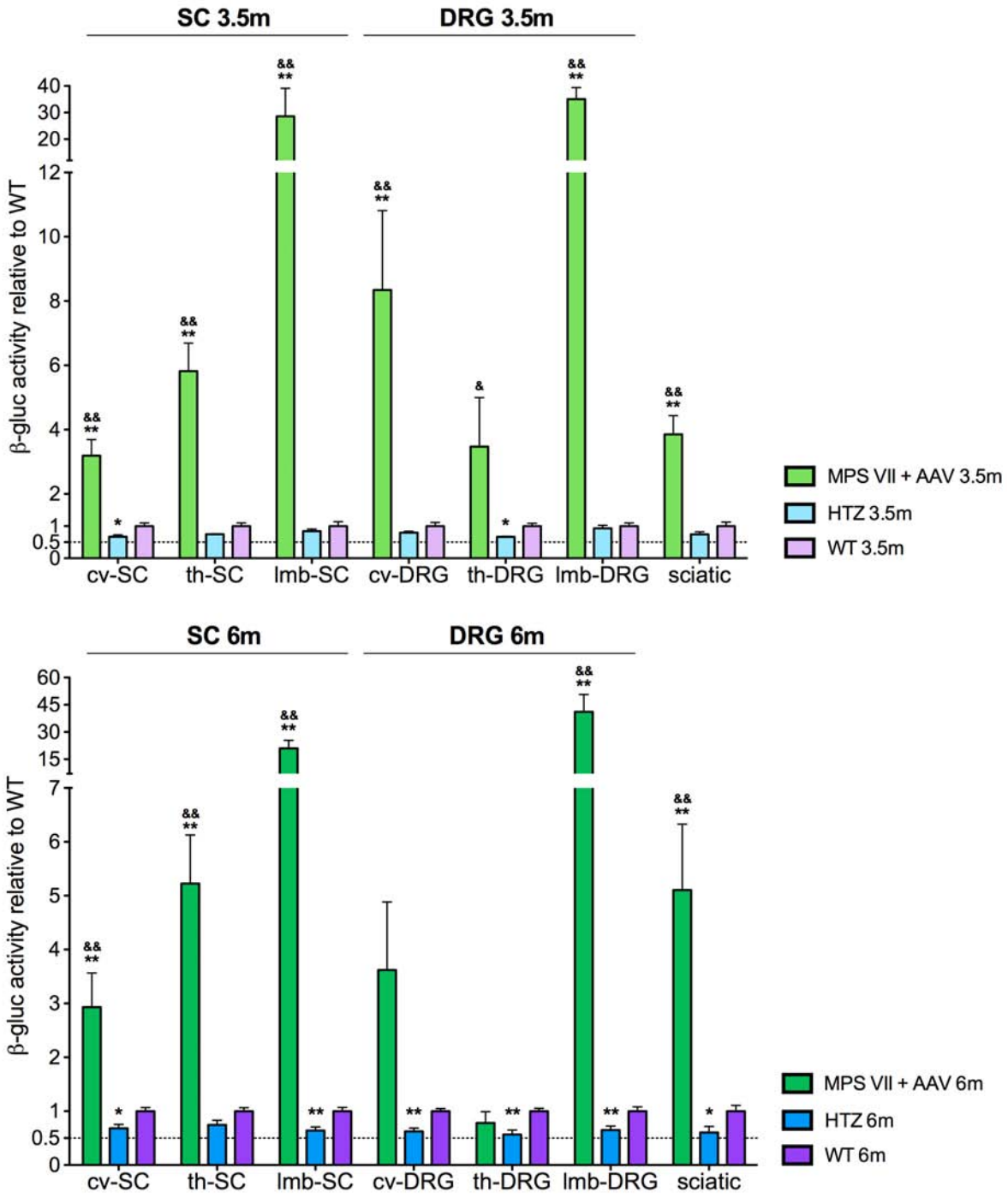

Figure 33: β-Glucuronidase activity in spinal cord (SC), dorsal root ganglia (DRG) and sciatic nerve expressed as ratios vs. WT mice. Statistical analysis by pairwise Mann-Whitney U tests. * vs. WT, & vs. HTZ. Sample sizes from *n* = 6 to *n* = 8. *cv*, cervical; *th*, thoracic; *lmb*, lumbar.

2.2.3.3. β-Hexosaminidase activity

As a biochemical marker of MPS VII disease, we analyzed the secondary elevation of β-hexosaminidase activity in samples of MPS VII, AAV-treated MPS VII, HTZ and WT mice. The evaluation was done for all the organs and areas that had previously been characterized for β-glucuronidase activity at both experimental time points, with the exception of sera. Omnibus statistical analysis of β-hex activity was performed by non-parametric Kruskal-Wallis tests, obtaining *p*-values smaller than 0.001 in all the cases, which revealed great overall differences among the four groups in all the areas analyzed for both treatment time points (data not shown). Subsequent Mann-Whitney U pairwise tests dissected the differences between experimental groups two by two (**Figures 34**, **35** and **36**).

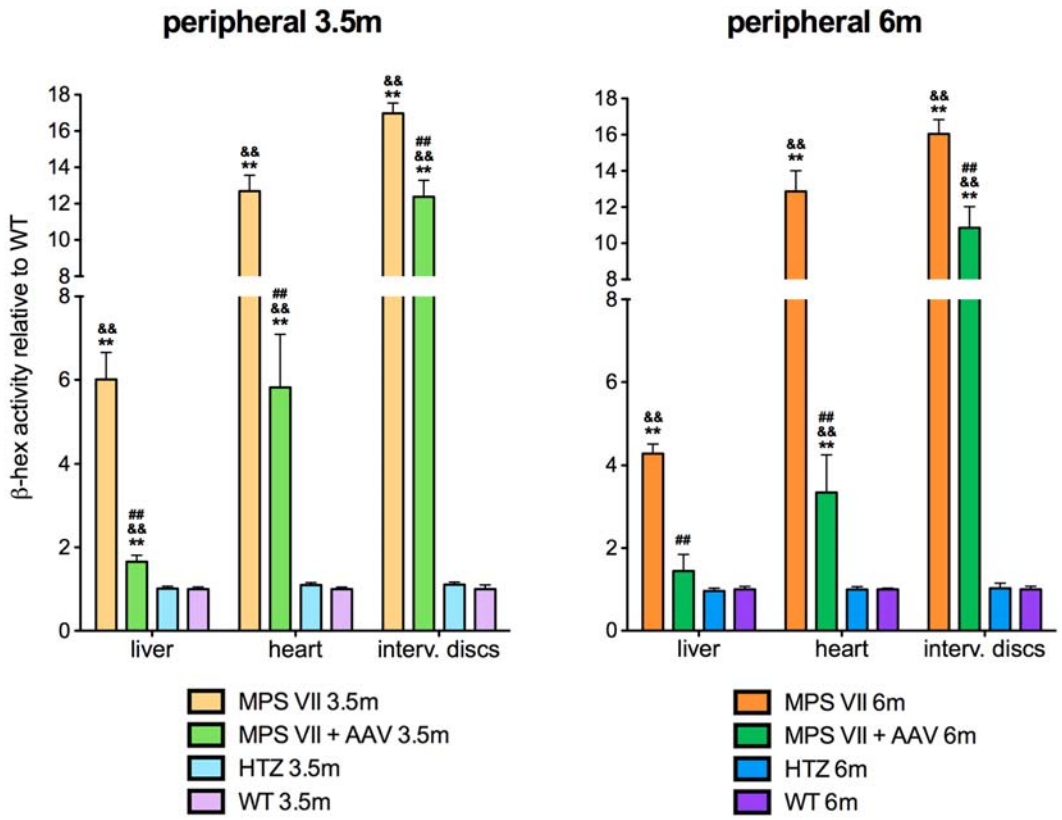

Figure 34: β-Hexosaminidase activity in peripheral organs and structures expressed as ratios vs. WT mice. Statistical analysis by pairwise Mann-Whitney U tests. * vs. WT; [&] vs. HTZ; [#] vs. MPS VII. Sample sizes from *n* = 6 to *n* = 8, except 6-month-old intervertebral discs, *n* = 4.

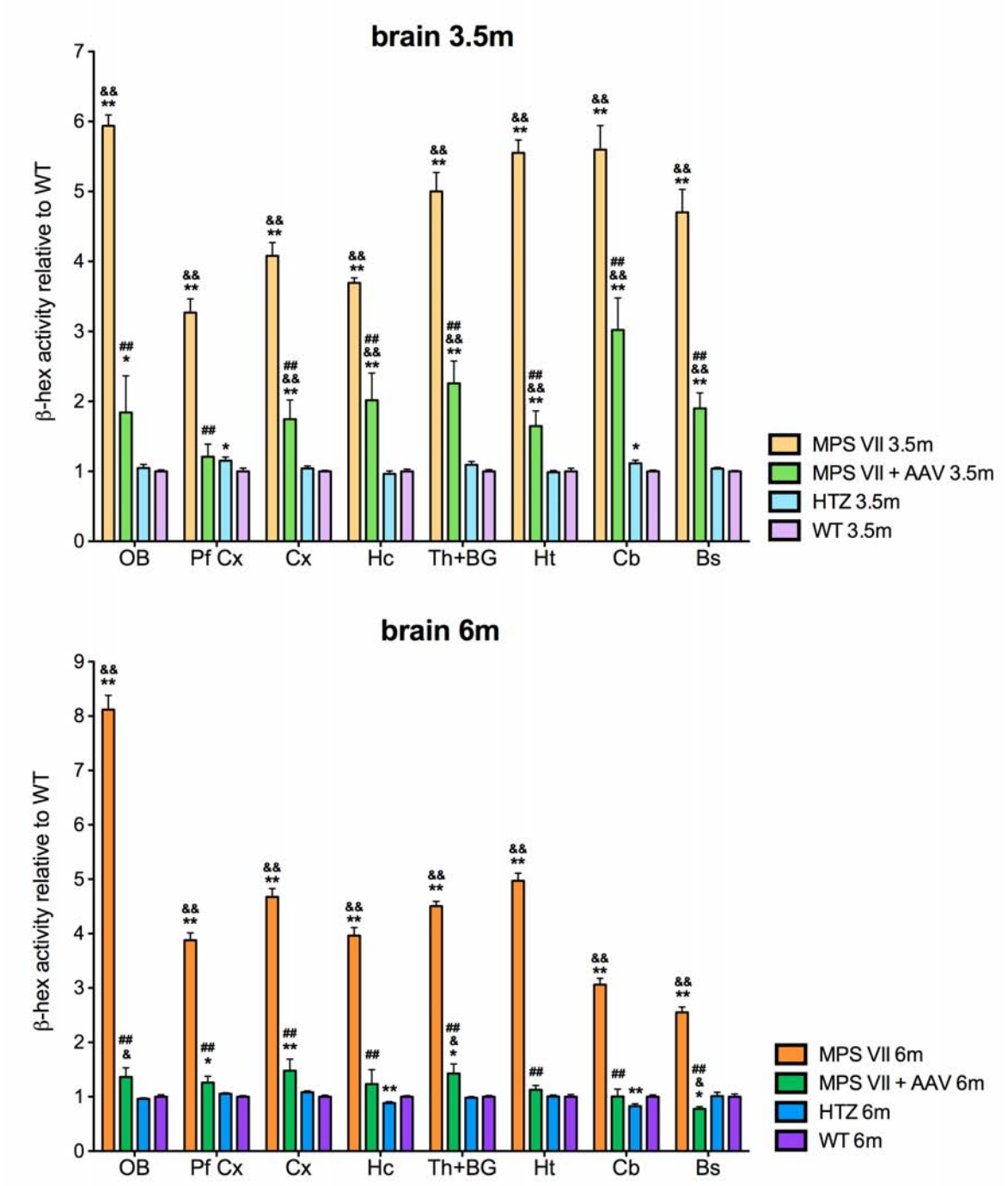

Figure 35: β-Hexosaminidase activity in brain structural areas, expressed as ratios vs. WT mice. Statistical analysis by pairwise Mann-Whitney U tests. * vs. WT; $^{\&}$ vs. HTZ; $^{\#}$ vs. MPS VII. Sample sizes from *n* = 6 to *n* = 8.

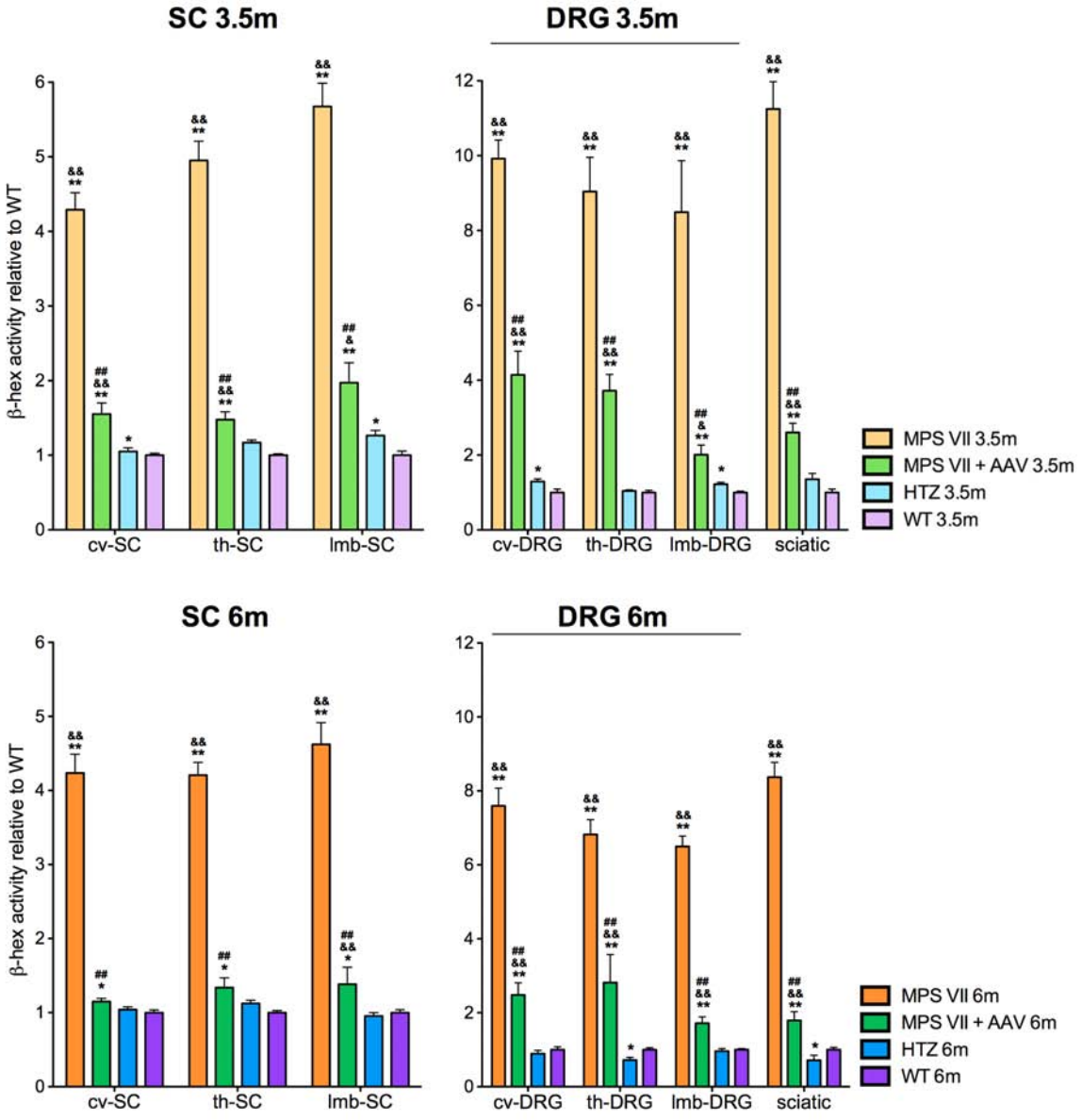

Figure 36: β-Hexosaminidase activity in SC, DRG and sciatic nerve, expressed as ratios vs. WT mice. Statistical analysis by pairwise Mann-Whitney U tests. * vs. WT; $^{\&}$ vs. HTZ; $^{\#}$ vs. MPS VII. Sample sizes from *n* = 6 to *n* = 8.

As it was expected, MPS VII mice show higher β-hex activity than WT and HTZ mice in all the areas analyzed. Since HTZ mice display normal phenotype, β-hex activity differences between HTZ and WT mice are not expected. However, the pairwise statistics between these groups reveal significant differences in several areas (as shown in **Figures 35 and 36**). As these differences are not consistent among time points and they are not expected, they are likely to be due to experimental variability.

Figures 34, **35** and **36** show that β-hexosaminidase activity of AAV-treated MPS VII mice is significantly lower than non-treated MPS VII mice in all the samples analyzed. Furthermore, in many of the tissues/areas analyzed, the decrease in β-hex activity reaches physiologic levels similar to those of WT and/or HTZ mice, which do not present MPS VII phenotype. Moreover, β-hex activity decreases over time in the AAV-treated group in all the areas analyzed, thus indicating the need of longer periods to achieve clearance of the accumulation of lysosomal surcharge in MPS VII mice (statistics not shown).

All together, these data demonstrate that the exogenous supply of β-glucuronidase obtained by intrathecal AAVrh10-GUSB injection is able to significantly decrease β-hexosaminidase activity of MPS VII mice in the nervous and somatic organs analyzed, reaching normal levels in some areas and confirming the biochemical correction or improvement of all the tissues analyzed.

2.2.3.4. LAMP-1 protein expression

LAMP-1 is a lysosomal membrane protein ubiquitously present in the cells. Since MPS VII is a lysosomal storage disease, we used LAMP-1 as a marker of lysosomal impairment and as a tool to describe the biochemical effect of the AAVrh10-GUSB treatment.

First, we performed LAMP-1 expression analysis in brain by immunofluorescence techniques. We analyzed cortex and hippocampus samples from MPS VII, AAV-treated MPS VII and HTZ mice by LAMP-1 immunofluorescence staining (**Figure 37 and 38**). We observed high LAMP-1 expression in non-treated MPS VII mice, whereas the AAV-treated mice displayed similar LAMP-1 pattern than HTZ mice at both ages, as it is shown in **Figure 37** for cortex samples and **Figure 38** for hippocampus samples.

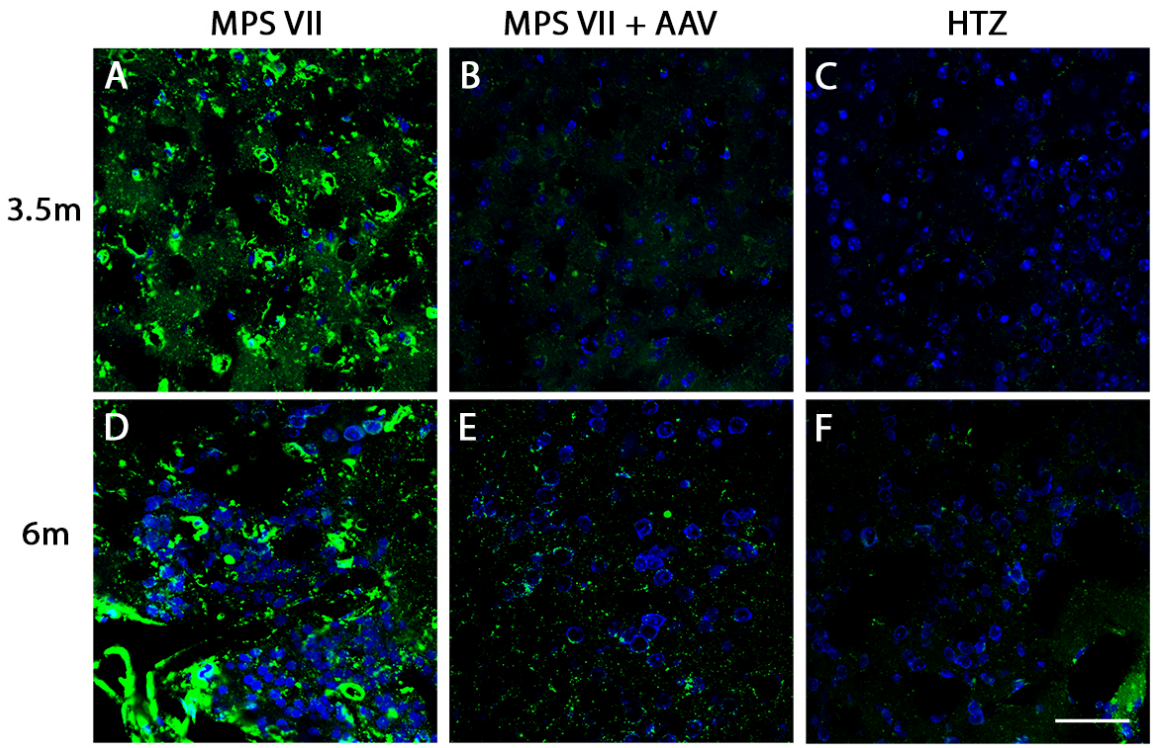

Figure 37: LAMP-1 immunofluorescence in cortex samples. LAMP-1 in green. Nuclei counterstaining in blue. Scale bar: 50 μm.

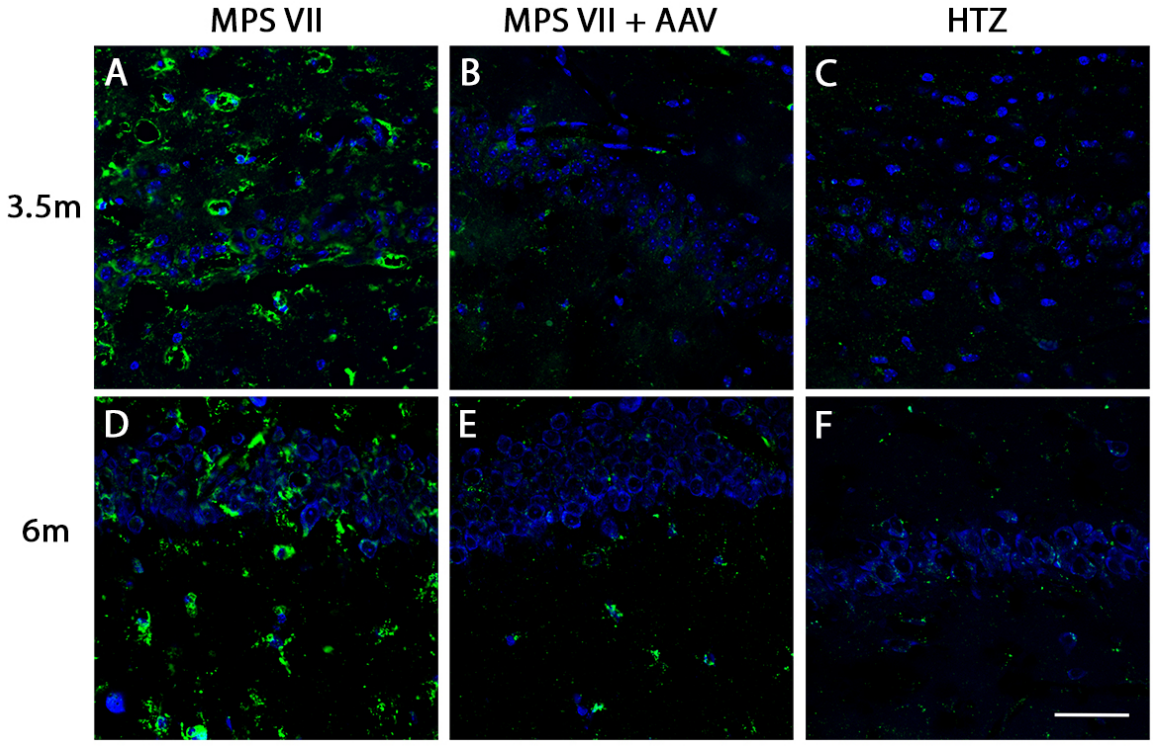

Figure 38: LAMP-1 immunofluorescence in hippocampus samples. LAMP-1 in green. Nuclei counterstaining in blue. Scale bar: 50 μm

Afterwards, we performed LAMP-1 expression analysis by western blot in order to quantify LAMP-1 expression in several somatic organs and nervous system areas. LAMP-1 is a 382-aminoacid protein that corresponds to about 42 kDa. Yet, the apparent size of LAMP-1 is 92 kDa because it is a highly glycosylated protein with 16 to 20 potential *N*-glycosylation sites that bind glycan chains in the endoplasmic reticulum. After processing of the oligosaccharides in the Golgi, LAMP-1 is converted to a family of mature forms of different sizes, ranging from 110 to 140 kDa (Andrejewski et al. (1999)).

In general, when comparing MPS VII to WT tissue by western blot, a significant difference was observed in all the tissues analyzed: while in WT tissue LAMP-1 appears as a 90 kDa band, MPS VII samples also display higher molecular weight bands. The size of these protein bands is different depending on the tissue analyzed and they are likely to be caused by differential glycosylation (**Figure 39**). Although we ignore the biochemical meaning of the presence or absence of these high molecular weight bands, we can use them as a marker of lysosomal impairment, in addition to the total amount of LAMP-1.

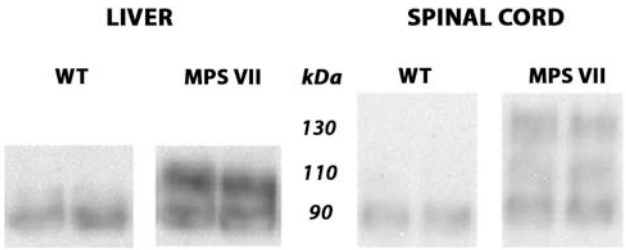

Figure 39: LAMP-1 western blot showing de differences in the band pattern between MPS VII and WT mice, in liver and lumbar spinal cord.

Some representative organs and nervous system areas were analyzed by LAMP-1 western blot: liver, heart, lumbar intervertebral disks, cortex, hippocampus, cerebellum and lumbar spinal cord. Blots were quantified and data are presented as ratios vs. WT in **Figure 40** for the somatic tissue samples and **Figure 41** for the nervous system samples. As stated before, two different quantifications were performed: the ratio between the high MW band vs. the low MW band (90kDa) in each sample (*high/low*), and the total LAMP-1 normalized by γ-tubulin in each sample (*total LAMP-1*). Data are not directly compared between ages because samples from

different experimental time points were analyzed in different WB. Statistical analysis was done by one-way ANOVA followed by Tukey *post hoc* test and results are depicted in **Figures 40 and 41**.

Figure 40: LAMP-1 western blot quantifications in somatic organs. *High/low*: ratio between high MW LAMP-1 and 90 kDa band. *Total LAMP-1*: total LAMP-1 vs. γ-tubulin. Sample size: *n* =

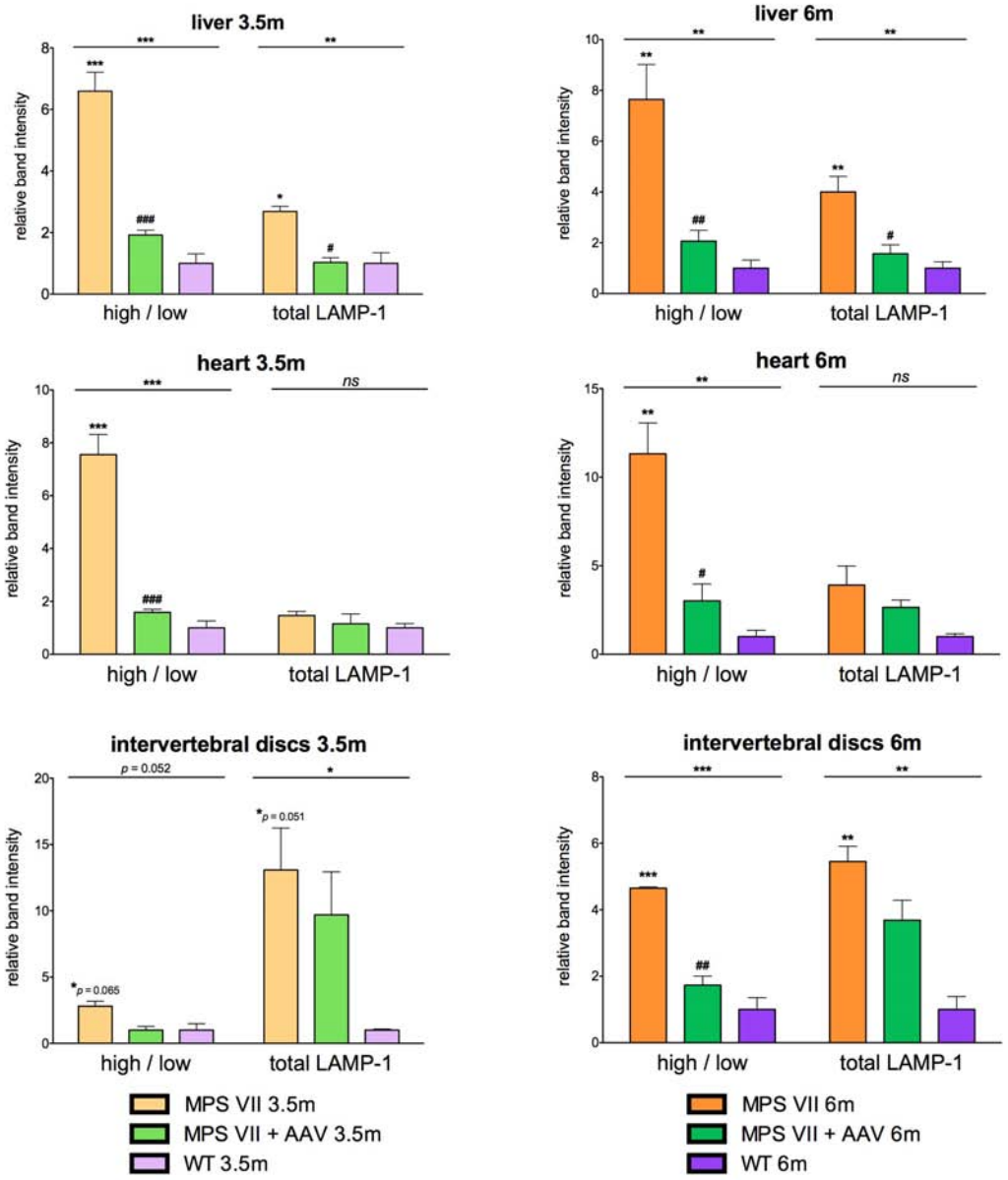

3 per group. Statistics: one-way ANOVA (depicted over the horizontal lines) and Tukey *post hoc*; * vs. WT; # vs. MPS VII.

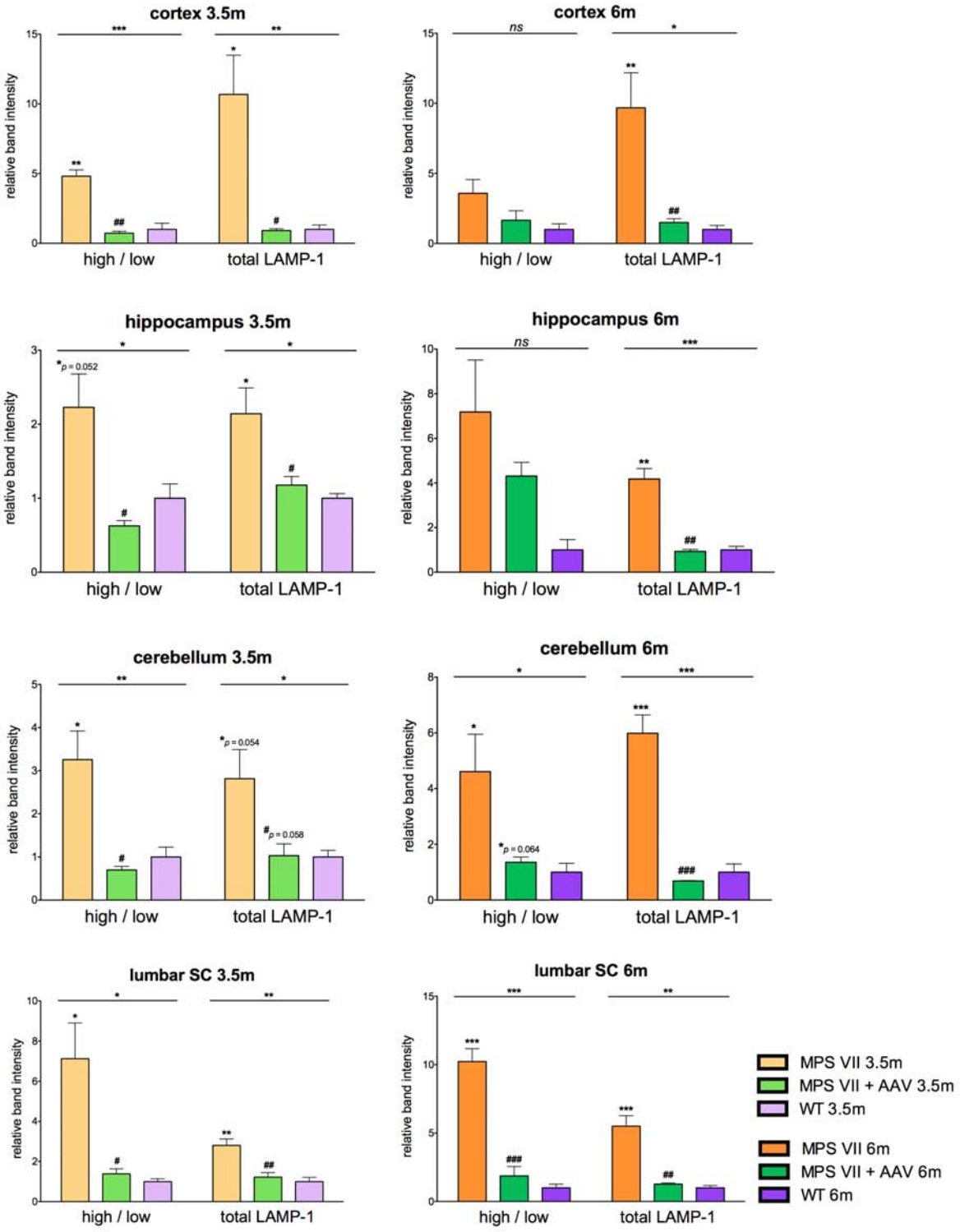

Figure 41: LAMP-1 western blot quantifications in nervous system areas. *High/low*: ratio between high MW LAMP-1 and 90 kDa band. *Total LAMP-1*: total LAMP-1 vs. γ-tubulin. Sample size: *n* = 3 per group. Statistics: one-way ANOVA (depicted over the horizontal lines) and Tukey *post hoc*; * vs. WT; # vs. MPS VII.

Results show that the ratio between high and low MW LAMP-1 bands was increased in MPS VII mice in all the areas analyzed. Restoring β-gluc activity with the AAVrh10-GUSB treatment was able to decrease this ratio to WT levels. Thus, the high MW band characteristic from MPS VII mice was decreased or it disappeared in all tissues from AAV-treated MPS VII mice, including heart and intervertebral discs. In several areas (3.5m-interv.discs, 6m-cortex and 6m-hippocampus), although presenting non-significant statistics, mean values showed the same tendency.

Besides, total LAMP-1 signal was increased in liver, IVD, cortex, hippocampus, cerebellum and lumbar SC of MPS VII mice at both time points. When treated with AAVrh10-GUSB, MPS VII mice decreased the total LAMP-1 to WT levels in all the areas except in IVD. Although no statistically significant differences in total LAMP-1 expression were found in heart samples, at 6 months of age there was an increase in the mean values of both MPSVII and AAV-treated mice, suggesting an alteration in total LAMP-1 that could not be reversed by the treatment. However, as stated before, heart samples showed a significant reduction in high/low LAMP-1 ratios.

In conclusion, LAMP-1 expression is altered in all the MPS VII tissues analyzed. The appearance of higher MW bands is characteristic of MPS VII mice and the treatment with AAVrh10-GUSB is able to correct it. Moreover, in most of the tissues analyzed, total LAMP-1 is increased in MPS VII mice respect to WT, and the treatment attains the normalization of LAMP-1 expression.

2.2.3.5. Relationship between biochemical results in AAV-treated MPS VII mice

As it is reported before in this work, samples from different AAV-treated mice show different β-glucuronidase activity levels, thus giving a wide variance between mice in the same tissue area (see Figures 31, 32 and 33). Moreover, β-hexosaminidase activity presents also great dispersion in data of samples from AAV-treated mice (see Figures 34, 35 and 36). In order to determine whether lower β-gluc activity could correlate with poorer biochemical correction, β-hex vs. β-gluc activity for each sample were compared between mice.

In general, we detected that mice with lower β-gluc tended to display higher β-hex in the majority of brain structural areas at both experimental time points. Besides brain, this relation was not found in any of the other areas and tissues analyzed: liver, heart, intervertebral discs, serum, spinal cord, DRG or sciatic nerve (data not shown).

As representative data of the mentioned relation in brain, **Figure 42** presents cortex and cerebellum correlations, which are brain areas displaying overall high and low β-gluc activity, respectively. Linear regression of the data of 3.5-month-old mice is more evident than that of 6-month-old mice. Enclosed in red appear the mice that present high β-hex activity correlating, although some exception, with low β-gluc activity. They are the mice labeled as 3.2, 3.6, 6.1, 6.5, 6.6 and 6.7.

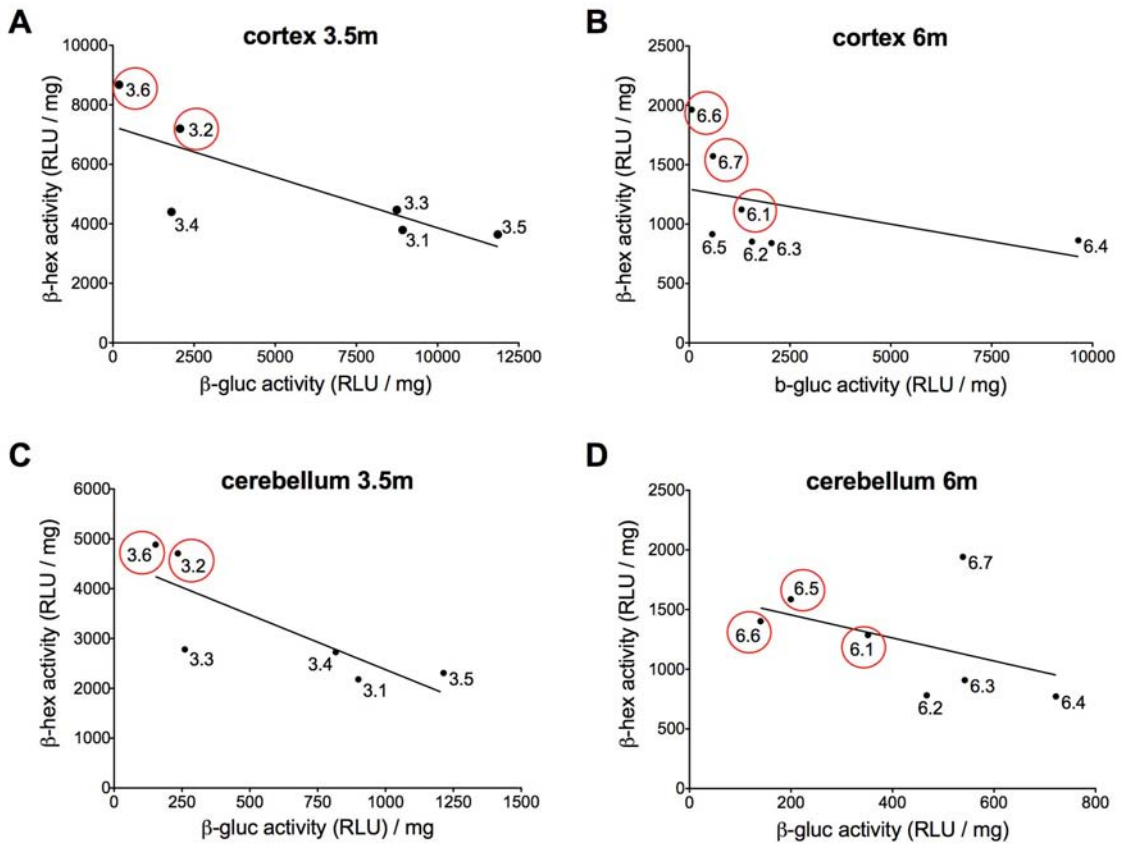

Figure 42: Correlation between β-gluc and β-hex activity of AAV-treated mice in cortex and cerebellum, with linear regressions. (**A**) Cortex of 3.5m old mice; $R^2 = 0.6264$ (**B**) Cortex of 6m old mice; $R^2 = 0.1979$. (**C**) Cerebellum of 3.5m old mice; $R^2 = 0.6361$ (**D**) Cerebellum of 6m old mice; $R^2 = 0.2006$. Numeric labels for mice identification. Red circles label low β-gluc correlating with high β-hex.

To further confirm the relationship between β-gluc activity and biochemical correction in brain, we compared LAMP-1 expression in cortex and cerebellum with the results presented in **Figure 42**. LAMP-1 quantifications of each AAV-treated mouse are presented in **Figure 43**, where higher values in any of the quantifications correspond to lower correction of the LAMP-1 alteration. The mice that presented high β-hex and low β-gluc activity in **Figure 42** have also been labeled in **Figure 43**, showing that these mice also display higher LAMP-1 expression and therefore less correction of the alteration.

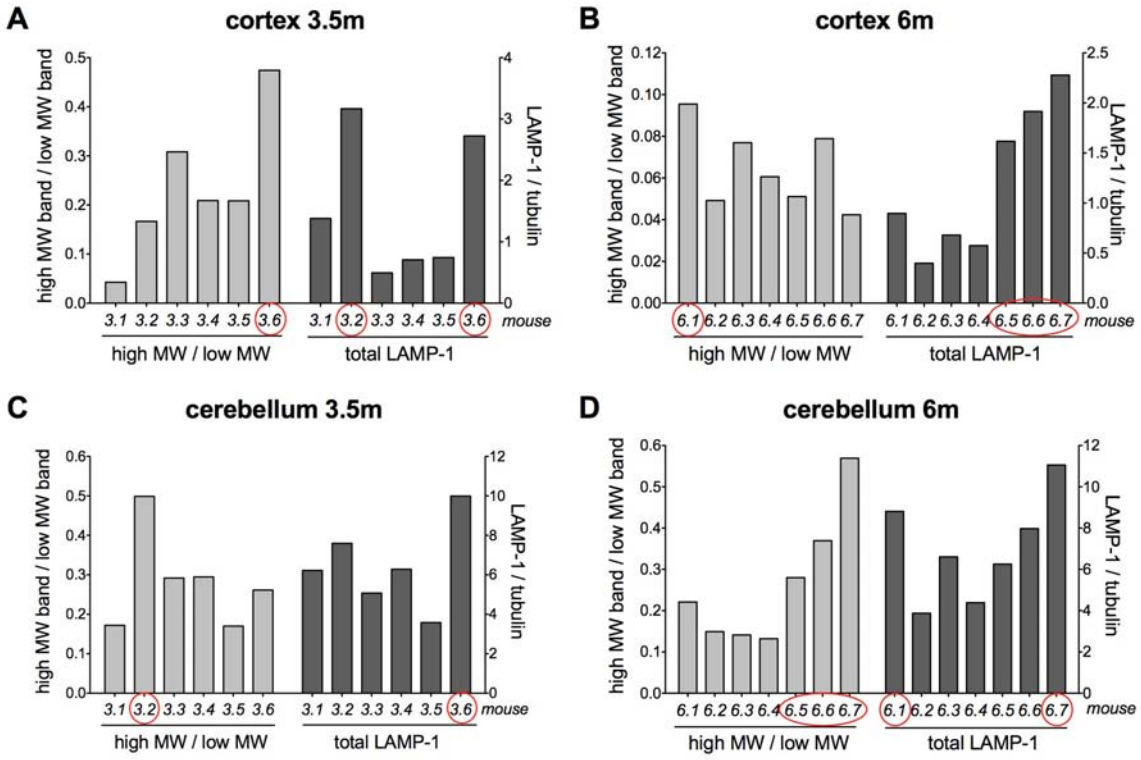

Figure 43: LAMP-1 expression quantification in AAV-treated MPS VII mice. Red circles labeling mice identified in **Figure 42** with low β-gluc and high β-hex activities when they correlate to high LAMP-1 quantification.

These results suggest that the β-gluc activity levels reached in brain by intrathecal AAVrh10-GUSB administration correlate with the biochemical correction attained, assessed by β-hex activity and LAMP-1 expression alterations.